Dear Editor,

Thank you for the time and sending us your decision. We have made responses and corrections to reviewers' comments and suggestions as shown below. Corrections made based on comments and suggestions are shown in red.

Reply to reviewer no. 1

We highly appreciate your time spent in reviewing the manuscript as well as your valuable comments and suggestions. We are glad that you are interested in our work and your positive feedback. Please find our line-by-line responses and corrections to your comments and suggestions. All responses, corrections and improvements are shown in red in the revised manuscript.

Reply to general comments
Thank you very much for pointing out these important issues. We totally agreed that the sensitivity and variability aspects of the source models and the bathymetry should be sufficiently discussed, Also, additional investigations should be applied to strengthen the conclusion related to tsunami wave trapping. In order to this, we have applied additional analyses mainly in **section 2.4, 2.5 and 2.6,** and related **sections 5.1**, 5.**2** and 5**.3.** In addition, to improve the clarity of the text, we have added more explanations to s**ection 2.3, 6.1, 6.2, 6.3,** as well as additional Tables and Figures to support the explanations. The manuscript was carefully re-written, and the English spellings were to our best to be improved. Please see more details below on our answers and responses.

Reviewer comments	**Our answers**	**Corrected manuscript**
Line 15: Please remove 'for the first time'	We thank the reviewer for pointing this out. We corrected it by removing the word.	**Line 14:** A small tsunami was generated, and recorded at tide gauge stations ~~for the first time~~.
Line 44: I suggest putting in a reference to Figure 1 already here.	We thank and agree with the reviewer. We corrected it by linking a reference to Figure 1.	**From line 48 to line 49:** The locations of Hengchun Peninsula and the epicenters of the successive earthquakes are shown in Figure 1.
Line 51: The Lay and Kanamori refence is general but the way the	We thank the reviewer for pointing this out. The sentence	**From line 50 to line 56:** The respective magnitudes of

sentence reads it sounds like the paper refers to this event. Please rephrase, and include a specific reference work (e.g. from seismology) that consider the 2006 event in particular.	was rephrased, and additional references about earthquakes doublet in seismological perspective of view were included.	these two earthquakes were suggested to be M_L = 7.0 (M_w = 7.0 in the Global CMT catalog) for the former, and M_L = 7.0 (M_w = 6.9 in the Global CMT catalog) for the latter. From seismological perspective of view, pairs of large earthquakes with equivalent rupture size and occurred in a similar spatial and temporal proximity were specified as doublet (Lay and Kanamori, 1980; Kagan and Jackson, 1999). Sharing comparable earthquake magnitudes, and very close epicenters and occurrence times, the successive earthquakes are referred as an event of doublet (Ma and Liang, 2008; Wu et al., 2009).
Line 51: 'Casualties', do you mean 'fatalities'? The former also refer to injuries, the latter only to loss of life.	Thank you very much for the suggestion. According to the report of National Disaster prevention and Protection Commission, R.O.C., 2007, the 26 December 2006 earthquakes caused 44 injuries, including 2 fatal ones, 3 building collapse, and massive damages of submarine communication cables. To that sense, we considered to use the vocabulary 'Casualties' here.	
Line 57: 'propagated toward' à 'propagated towards'	We are very sorry for making this spelling mistake. We	**Line 61:** A small tsunami was generated

	corrected it.	after the successive strong motions of these earthquakes. The tsunami propagated towards, and reached the western coast of southern Taiwan immediately after the earthquakes.
Line 60: Rephrase sentence, my suggestion 'as it was rare because it was generated by earthquakes in short succession'.	We thank and agreed with the reviewer. We corrected it by rephrasing the sentence.	**Line 64-66:** The December 2006 tsunami was an important event and attracted public interest, as it was rare because it was generated by earthquakes in short succession, and was a new issue among social communities and ordinary persons in Taiwan about tsunamis.
Line 62: 'heightens' à 'increased'	We thank the reviewer for pointing this out. We corrected it.	**Line 67:** This recent tsunami not only corroborates the tsunami risk in Taiwan, but also increased the awareness of disaster risk management, such as preparedness, and mitigation countermeasures for the next tsunamis.
Line 65: Several repeats of the above in this paragraph, I suggest shortening.	We thank the reviewer for pointing this out. We shortened the paragraph.	Please see **line 69**. The tsunami observations reported following the 26 December 2006 tsunami also opened some questions.
Line 67: Please delete sentence starting with 'It has been common understanding…'. This can certainly be disputed and the scientific community is	We thank the reviewer for pointing this out. The sentence starting with 'It has been common understanding…' have been deleted, and the sentences	**Line 70:** First, the first tsunami wave crest was not shown as the largest in some stations.

definitely aware that later wave arrivals can be larger than the first.	were rephrased.	
Line 71: 'prolonged'? Prolonged compared to what?	We apologize for our confusing expression. We meant that some stations recorded the tsunami durations for more than 6 hours during the 2006 earthquake tsunami. We have removed the word 'prolonged', and rephrased the sentence to improve the lack clarity.	**Line 72 to line 73:** Second, tsunami durations for more than 6 h were recorded at some stations following the earthquakes.
Lines 80-81: Something is missing in these statements, please rephrase so the meaning is more apparent.	We thank the reviewer for pointing this out. We rephrase the sentences and the meaning.	**Please see line 77-88** The other issue was that which source models could better explain the successive tsunamis to the recorded observations in southern Taiwan. Wu et al., 2008 simulated the tsunami from this event using single fault models. They numerically computed the tsunami propagation on a nested grid system with finest grids of 0.125 min resolution bathymetry data and compared their results with observation data from tide gauge stations. Although the source models to this tsunami event have been specified and modeled in previous study, the uncertainty and variability aspects of the source models and bathymetry have not been investigated thoroughly. Such uncertainties in earthquake fault parameters and significant

		difference among the open-source bathymetries can exaggerate the modeled results rather than the predictions from previous study to the 2006 tsunami. Therefore, it is critical to discuss such model's performances from viewpoint of sensibility perspective because it is desirable to obtain a tsunami source model and to understand the reliability of bathymetry data utilized for numerical simulation for reasonably estimating the tsunami wave activities during the 2006 tsunami.
Line 91: 'justify' à 'hindcast'	We thank the reviewer for pointing this out. We rephased the sentence.	**Line 98 to line 101:** The December 2006 earthquake tsunami represents a unique and recent incident in Taiwan; therefore, these findings could not only help further clarify tsunami generation and the important behaviors responsible for tsunami hazards facing the island of Taiwan but also have implications for tsunami warning and disaster risk management.
Line 99: Please delete 'In general', and replace the statement 'possible method to study' with 'one source of information we can use to study'. The point is that it can only be supplementary to other methods,	We thank and agreed with the point of view of the reviewer. We corrected it by rephrasing the sentence.	**Line 105 to line 106:** Time history data of sea levels recorded at coastal sites provide one source of information that we can use to study tsunami patterns.

it is usually not enough by itself.		
Line 112: 'represent the duration' à 'represent the observation' (duration written twice in sentence)	We thank the reviewer for pointing this out. We corrected it.	**Line 118:** The tsunami durations represent the observation time of high-energy tsunami waves persisting in a coastal site of observation.
Line 113: Remove 'of observation'. 'duration' à 'durations', and 'was' à 'were'	We thank the reviewer for pointing this out. We corrected it.	**Line 118 to line 121:** The tsunami durations represent the observation time of high-energy tsunami waves persisting at a coastal site. The tsunami durations at all the stations were identified based on a calculation of root mean square (RMS) sea levels, indicating the elapsed time of the wave amplitude above the normal oscillation level before the tsunami wave arrived (Heidarzadeh, 2021).
Line 127: 'The' Fourier analysis …	We thank the reviewer for pointing this out. We corrected it.	**Line 132-136:** The Fourier analysis and the wavelet (time-frequency) analysis. The Fourier analysis is based on the fast Fourier transform (FFT) algorithm, applied based on the updated open-source library Numpy in the Python package (Harris et al., 2020). The Fourier analysis was performed to estimate the spectral components of the time history data of the tsunami waveform.
Line 137: 'the' wavelet analysis …	We thank the reviewer for pointing this out. We corrected it.	**Line 133:** The Fourier analysis and the wavelet (time-frequency)

		analysis.
Line 144: The first sentence in the paragraph is somewhat misleading. I would rather say it is a computer-based method describing the equations of motion for the tsunami wave propagation. You could also add that there are various methods, but that the shallow water model is most used, although dispersive models are more and more used as well.	Thank you very much for the valuable comments. We rephrased it to improve the clarity of the numerical methods.	Please see **section 2.3 (from line 149-177)**
Line 149: I would say that TUNAMI also cover far-field tsunamis, with limitations of course.	Thank you very much for the valuable comments. We add additional information to this part.	Please see **section 2.3 (from line 149 to 177)**
Line 155: You do not describe mesh refinement anywhere. How do you ensure convergence? What is your grid resolution, and what exactly is the CFL number? It should be a minimum to test convergence at least with two different (optimally three) mesh sizes.	We simulated the tsunami propagation using a 450 m bathymetric grid. The mesh size in x and y directions are 538 and 631. The CFL condition is presented as: $\Delta t \leq \frac{\Delta x}{\sqrt{2gh_{max}}}$ Where the Δt is the time interval, Δx is the grid spacings, and h_{max} is the maximum water depth in the model domain.	Please see **section 2.3 (from line 149 to 177)**
Line 160: You have stated this before. I suggest to delete this sentence that only repeats what is already written in the intro.	We thank and agreed with the reviewer. We deleted the sentence.	
Line 168: Are you simulating with uniform slip? Could you gain anything with adding non-	Thank you very much for the valuable suggestions. The tsunami sensitivity to non-	For the approach, please see section 2.4.2 (**from line 220 to 248**) and for the results of

uniform slide and simulate different realisations of the slip distribution? This deserves to be discussed more.	uniform fault slip distribution is evaluated.	sensitivity analysis, please see section 5.2 (**from line 464 to 478**)
Line 186: 'horizontal effect' à 'horizontal deformation contribution to tsunami generation'	We appreciated the reviewer for the correction. The sentence was revised.	**Please see line 175-176:** The horizontal deformation contribution to tsunami generation on the steep bathymetric slopes (Tanioka and Satake, 1996) was included.
Line 191: Why could this not have been caused by landslides? Please elaborate / substantiate, or otherwise skip this statement if you cannot back it up more explicitly.	The statement was skipped.	
Line 193: Add 'simulated' before 'initial'.	The vocabulary was revised.	**Please see line 173-174:** As the simulated initial condition inputted for numerical tsunami simulation, the initial water level distribution is calculated from the earthquake fault parameters using the theory of Okada, 1985.
Line 203: You may need to elaborate what you mean by 'two bathymetric scenarios'. You probably mean tsunami simulations applying two different bathymetries. You may motivate your work by mentioning how wrong the open source bathy was for 2018 Palu. Similar for 2018 Anak Krakatoa (e.g. Zengaffinen et al., 2021).	For the bathymetric scenarios stated here, we meant the actual and manipulated bathymetries used in numerical simulations to examine the how bathymetry can influence the tsunami wave directivity and wave trapping. In addition, the variability aspects of open source bathymetry to model results was examined.	For the clarity of bathymetric scenarios, please see **section 2.6 (from line 276 to 291).** The details of actual and manipulated bathymetries used in numerical simulations were summarized in **Table 5**. For the examination of tsunami sensitivity to open source bathymetry, the 2018 Palu and the 2018 Anak Krakatoa tsunami were referred as backgrounds

		and the approach and results could be found in **section 2.5 (from line 250 to 274)** and **section 5.3 (from 480 to 502)**, respectively.
Line 207: Both are scenarios in a way. I would rephrase, and rather say 'manipulated bathymetry' rather than 'hypothetical scenario'.	We appreciated the reviewer for the comments. The sentences were rephrased.	Please see **section 2.6 (from line 276-291)**.
Line 211: You only investigate two different bathymetries, and this might be a bit thin to conclude in general. I suggest that the uncertainty related to the bathymetry is discussed more.	Thank you very much for the valuable suggestions. We agreed with the reviewer. In addition to the two different bathymetries (i.e., actual and manipulated bathymetry by replacing sea depths larger than 500 m to 500 m), a rather hypothetical situation was examined using the manipulated bathymetry of flatted sea bottom of 500 m depth.	Please see **section 2.6 (from line 276-291)** and **section 6.1 (from line 505-535).**
Line 231: Please rephrase 'different mechanism of tsunami waves was' à 'different propagation effects were'	We appreciated the reviewer for pointing this out. The sentence was revised.	**Please see line 307 top line 308:** These results suggest that the different propagation effects were active at these coastal sites during the passage of the 2006 tsunami.
Line 237: The aspects of the wave recordings should be move more up front, at least within this subsection, it is important background.	We appreciated the reviewer for the valuable comments. The aspects of the wave recordings were moved and considered as important background for simulating scenarios with non-uniform fault slip distributions.	**Please see line 455-462.** While the single fault models can produce the simulated tsunami waveforms well consistent to the observations, the badly sampled (i.e., 6 min interval) signals recorded in coastal stations also raise some

		questions, as one would expect some potential high tsunami waves behind the observed signals. To that sense, overestimation of modeled results was expected, but the simulated tsunami waveforms using single fault models present the opposite. This indicates that the single fault models (i.e., with uniform fault slip) may not be sufficient and the asperity area (i.e., with large fault slip) on the fault should be evaluated. The tsunami sensitivity to asperity locations of multiple fault models will be discussed in next section.
Line 254: You say 'abnormally long', but compared to what?	We apologize for our confusing expression. We meant that Kaohsiung and Houbihu station recorded the tsunami durations for more than 6 hours during the 2006 tsunami. We have removed the word 'prolonged', and rephrased the sentence to improve the lack clarity.	**Please see line 326-328** The calculated tsunami duration at Dongkung was as much as 3.9 h, while the tsunami continued for more than 6 h in Kaohsiung and Houbihu.
Line 271: What does the background spectra contain? Are they de-tided? Please clarify.	We apologize for our lack expression. The background spectra are the spectral components calculated from de-tided observed data of 5 h before the tsunami arrival.	**Please see line 346 to line 350** The background spectra are the spectral components calculated from de-tided observed data of 5 h before the tsunami arrival, and the spectral components of the observed tsunami waveform were computed using 5 h data recorded at tide gauge after

		tsunami wave arrived.
Line 293: I think this is stating the obvious, and it could perhaps be skipped?	Thank you very much for pointing this out. We skipped this statement.	
Line 329: 'determined' à 'estimated'	Thank you very much for pointing this out. The vocabulary was revised.	**Please see line 388** Assuming the mean sea depths around tsunami source region is 300 m, the fault rupture dimensions for the two earthquakes could be estimated to 20- 40 km.
Line 372: I would say it is the opposite: The data can be used to validate the numerical simulations.	Thank you very much for the valuable comments. The sentence was rephrased.	**Please see line 181-184** Multiple forward tsunami simulations were conducted using single fault models with different fault depths and fault orientations. The main goal of the multiple forward tsunami simulations was to find a single fault model that could produce tsunami waveforms that were highly consistent with the tide gauge station observations in southern Taiwan.
Line 377: If there is undersampling, you would normally expect the numerical simulations to overestimate the wave measurements, because the measurements would miss out on larger amplitude waves. Here it seems to be the other way around, implying that the simulations are lower than you would expect from the	We appreciate the reviewer for the valuable suggestions on this issue. We established and simulated the non-uniform slip scenarios to examine whether the measurements have missed out on larger amplitude waves.	**Please see section 2.4.2 (from line 220 to 248) for the approach and section 5.2 (from line 464 to 478) for the results.**

measurements. The authors need to elaborate on this. For instance, why was not alternative scenarios or random / heterogeneous slip investigated with several scenarios?		
Line 388: Replace 'It is commonly understood that' with 'The longest wave component'. Then add an 'a' ahead of 'velocity'.	Thank you very much for the valuable comments. The vocabulary was revised, and sentence was rephrased.	**Please see line 499** The longest wave component of tsunami travel with a velocity that is mainly governed by seafloor depths.
Line 390: Add 'through diffraction' after 'wave direction'.	We appreciate the reviewer for the correction. The vocabulary was added.	**Please see line 507 to 508** The significant change in propagation speed allows the tsunami to change its wave direction through diffraction.
Line 391: 'of the' à 'using'	Thank you very much for the suggestion. The vocabulary was revised.	**Please see line 511 to line 512** Simulated snapshots of tsunami wave propagation using actual (MS) bathymetry are shown in Figure 21.
Line 395: I found it difficult to follow the authors in this paragraph. I suggest that the authors review the text and try to rephrase it, at least the first 6-7 lines.	We apologize for the confusing expression in this paragraph. The paragraph was re-written.	Please see **section 6.1 (from line 505 to 535).**
Line 422: I suggest to comment on previous studies investigating fits and misfits using open source bathymetry and topography data, e.g. Griffin et al., (2015).	Thank you very much for this valuable suggestion. We examined the misfits of modeled results using open-accessible bathymetry and topography.	Please see **section 5.3 (from line 480 to 502)**
Line 426: The sentence starting with 'These results further confirmed …' I found was	We appreciate the reviewer for the valuable comments. To strength the conclusion related to	Please see **section 6.2** and **6.3 (from line 537 to 573)**

formulated too conclusive. The number of investigations are rather limited, and there should be room for additional investigations to strengthen the conclusion related to wave trapping.	wave trapping, we applied additional analysis including energy trapping ratio, and the comparison of calculated waveforms.	
Line 439-441: What the authors write here is not clear from the figures. If there is additional not shown that back this up please state this explicitly.	We apologize for the unclarity of the figure. We replotted the figure and rephased the statement in this paragraph.	Pease see **section 6.4 (from line 575 to 608)** and **Figure 27.**
Line 482: 'characterized' à 'analyzed'	Thank you very much for the suggestion. The vocabulary was revised.	Please see line 617 The physical characteristics of tsunami waveforms in all three tide gauge stations in southern Taiwan during the December 2006 tsunami were analyzed.

2.3 Numerical tsunami simulation

Numerical simulation is a computer-based method that describes equations for the motion of tsunami wave propagation. Tsunami wave propagation can be numerically modeled based on various theories, including shallow water and dispersive wave theories. Among those theories, the shallow water equations are some of the most commonly used methods to model tsunami propagation from the source to nearshore areas. Various computational models have been developed to solve shallow water equations, and the TUNAMI (Tohoku University Numerical Analysis Model for Investigation of tsunamis) code is one of the widely used models to numerically simulate both far-field and near-field tsunamis (Suppasri et al., 2010; Suppasri et al., 2014). The second version of the TUNAMI code (TUNAMI-N2) was mainly developed to deal with near-field tsunamis by applying the nonlinear theory of shallow water equations, which is solved using a leap-frog scheme (Imamura, 1995). Since the 2006 tsunami presented as a near-field tsunami in Taiwan, the TUNAMI-N2 model was used in this study to simulate the 2006 tsunami with nonlinear shallow water equations. The nonlinear shallow water equations on the Cartesian coordinate system are presented in equations (2)-(4), and the nonlinear equations are solved by applying the finite difference method:

$$\frac{\partial \eta}{\partial t} + \frac{\partial M}{\partial x} + \frac{\partial N}{\partial y} = 0 \tag{2}$$

$$\frac{\partial M}{\partial t} + \frac{\partial}{\partial \chi}\left(\frac{M^2}{D}\right) + \frac{\partial}{\partial y}\left(\frac{MN}{D}\right) + gD\frac{\partial \eta}{\partial \chi} + \frac{gn^2}{D^{\frac{7}{3}}} M\sqrt{M^2+N^2} = 0 \tag{3}$$

$$\frac{\partial N}{\partial t} + \frac{\partial}{\partial \chi}\left(\frac{MN}{D}\right) + \frac{\partial}{\partial y}\left(\frac{N^2}{D}\right) + gD\frac{\partial \eta}{\partial y} + \frac{gn^2}{D^{\frac{7}{3}}} N\sqrt{M^2+N^2} = 0 \tag{4}$$

In these equations, η is the water level, M and N are the discharge fluxes in the x and y directions, respectively, D is the total water depth, g is the gravitational acceleration, and n is Manning's roughness coefficient. The bottom friction term was represented by the Manning roughness coefficient, which was set as 0.025 s $m^{-1/3}$, assuming that the seafloor in the model domain is in perfect condition. The numerical tsunami simulations were conducted with a time interval of 0.1 s and grid intervals of 450 m. The entire model domain covered the source region and southern Taiwan, which comprised mesh numbers of 538 and 631 in the x and y directions, respectively. The time interval and grid intervals were set up to satisfy the Courant–Friedrichs–Lewy (CFL) condition to ensure the stability of the simulation. The CFL condition is presented in equation (5):

$$\Delta t \leq \frac{\Delta x}{\sqrt{2gh_{max}}} \tag{5}$$

where Δt is the time interval, Δx is the grid spacing, and h_{max} is the maximum water depth in the model domain. As the initial condition inputted for numerical tsunami simulation, the initial water level distribution was calculated from the earthquake fault parameters using the theory of Okada (1985). In addition, the horizontal deformation contribution to tsunami generation on steep bathymetric slopes (Tanioka and Satake, 1996) was included. The calculation conditions for the numerical tsunami simulation are summarized in Table 1.

2.4 Sensitivity analyses of source models

2.4.1 Single fault models

Multiple forward tsunami simulations were conducted using single fault models with different fault depths and fault orientations. The main goal of the multiple forward tsunami simulations was to find a single fault model that could produce tsunami waveforms that were highly consistent with the tide gauge station observations in southern Taiwan.

There were two moment tensor solutions available from the Global Centroid Moment Tensor (GCMT) Project and United States Geological Survey (USGS) for the successive earthquakes on 26 December 2006 (Figure 2.). Each solution suggested two possible fault planes for those earthquakes. The focal mechanisms for the two earthquakes estimated by the GCMT and USGS are summarized in Table 2.

Through the analysis of the tsunami waveforms simulated by the multiple forward tsunami simulations, one of those fault planes could be chosen as the appropriate fault plane for the respective earthquakes of the 2006 earthquake doublet. A similar approach has been applied in a previous study to obtain the optimum fault plane for the 2016 Fukushima normal faulting earthquake (Gusman et al., 2017).

Wu et al. (2008) computed synthetic tsunami waveforms based on single fault models using different fault planes of the GCMT solutions. They found that the nodal plane (NP) of NP2 of the first earthquake, with a strike of 329°, dip of 61°, and rake of -98°, and the fault plane of NP1 for the second earthquake, with a strike of 151°, dip of 48°, and rake of 0°, produced tsunami waveforms that better fit the observed data.

Based on the study conducted by Wu et al. (2008), the focal mechanisms of NP2 to the first earthquake and NP1 to the second earthquake from the GCMT solution were used for a sensitivity analysis of fault depths. An approximated fault area with a 40 km length and a 20 km width (800 km^2) was estimated for the successive earthquakes based on the empirical formula with tsunami source periods. The methods by which the fault area of the two earthquakes was obtained are discussed in section 4.1. For the given moment magnitude (M_w) values of the 7.0 and 6.9 earthquakes, the amount of average slip can be estimated to be 1.66 m for the first earthquake (i.e., M_w 7.0) and 1.17 m for the second earthquake (M_w 6.9), assuming a rigidity of 30 Gpa. The centroid depths of the GCMT (20 km) and USGS (25 km) solutions for the first earthquake are significantly different, while a similar depth of 33 km was estimated from both solutions for the second earthquake. Therefore, for the sensitivity analysis of central fault depth, the central fault depths of 15, 20, 25, and 35 km of the first earthquake were evaluated.

After determining the best central fault depth for the single fault models of the two earthquakes, multiple tsunami forward simulations were applied to all possible fault planes from the moment tensor solutions estimated by GCMT and USGS using a single fault. The misfit of observed and simulated tsunami waveforms from the multiple tsunami forward simulations was calculated and compared to examine the focal mechanisms that better explain the observed tsunami data. The misfit of the observed and simulated tsunami waveforms can be calculated using equation (6):

$$\varepsilon = \frac{1}{N}\sqrt{\sum_{i=1}^{N}\frac{(Obs_i - Sim_i)^2}{(Obs_i)^2}} \qquad (6)$$

where ε is the misfit of the observed and synthetic tsunami waveforms, N is the total number of data points, Obs_i is the observed data at time step i, and Sim_i is the simulated data at time step i. Equation (8) calculates ε for one station. For cases with several stations, the overall misfit is obtained from the mean of the ε values computed from all the stations.

2.4.2 Multiple fault models

After determining the best central fault depths and fault orientations of a single fault, the area of each single fault was subdivided into 8 subfaults with areas of 10 km × 10 km, with 4 and 2 subfaults along the strike and dip axes, respectively. The locations of each subfault in the fault model of the two earthquakes are shown in Figure 4. The top depths for the two earthquakes are 15.3 km and 29.1 km, which correspond to subfaults 1-4 in each fault model (Figure 4a, b). The rest of the depths from the shallowest to the deepest portion along the dip axis are derived using fault parameters of width dimensions and dip angles. The respective fault parameters of each subfault in the fault models of the two earthquakes are summarized in Table 3.

The tsunami sensitivity to the non-uniform slip distribution of the fault model was evaluated. For that purpose, two slip levels for each subfault were established, namely, the large (asperity) slip and the background slip region of the entire fault. The large slip and background slip region should satisfy the M_w to avoid overestimation. The slip amount in each region was obtained using the following procedures. First, the amount of average slip (D_a) was calculated using the M_w, the entire fault area (S), and a rigidity (μ) of 30 GPa, per the equations introduced by Kanamori (1977):

$$M_w = \frac{\log M_0 - 9.1}{1.5} \qquad (7)$$

$$D_a = \frac{M_0}{\mu S} \qquad (8)$$

Next, the amount of large slip ($2D_a$) was assumed to be twice that of the average slip based on a 2017 tsunami receipt report. The total area of the large slip area (S') was set to be 25% of the entire fault area, and the seismic moment of the large slip area (M_0') can be obtained using equation (8). Then, the slip amount of the background area (D_b) can be estimated using the area of the background region (S_b) following equations (8)-(9):

$$S_b = S - S' \qquad (8)$$

$$D_b = \frac{M_0 - M_0{}'}{\mu S_b} \quad (9)$$

The details of the slip amount in each region for the two earthquakes are summarized in Table 4a.

After determining the slip amount of the asperity and background regions, the tsunami sensitivity to the asperity location was studied. The asperity area with the large slip was located in the shallow portion of the entire fault area based on information from the 2011 Tohoku-Oki earthquake (Satake et al., 2013; Fukutani et al., 2021), focusing on the north (subfaults 3-4), central (subfaults 2-3), and south (subfaults 1-2) parts of each earthquake fault model. Assuming different asperity locations for the two earthquakes, a total of 9 scenarios were simulated. The multiple fault models and the generated tsunamis of each earthquake are shown in Figures 5 And 6. The asperity locations of multiple fault models for the two earthquakes in each scenario are summarized in Table 4b.

2.5 Tsunami simulation using open-source bathymetry data

In addition to the fault parameters of the source models, bathymetry data are needed for simulating tsunami wave propagation. Simulated tsunami propagation results are known to be sensitive to the accuracy and resolution of bathymetry data. Although it can be expected that bathymetry data with a higher accuracy and resolution can produce simulated results that better fit the actual values, such data are not always available and freely accessible. Due to this limitation, open-source datasets have often been utilized for modeling tsunamis in many previous studies (Koshimura et al., 2008; Suppasri et al., 2012; Li et al., 2016; Otake et al., 2020).

Unfortunately, open-source datasets are sometimes problematic and insufficient for the accurate simulation of tsunami waves because they lack accurate, quality data (Griffin et al., 2015). A similar issue has been reported by Zengaffinen et al. (2021) and Heidarzadeh et al. (2019) in simulating the 2018 Anak Krakatoa tsunami and the 2018 Sulawesi tsunami. Significant differences in various sources of datasets can also result in modeled results that contrast estimated values from previous studies. Therefore, for the purpose of tsunami hazard assessment, it is important to assess and note different available open-source bathymetries in relation to model performances, using the 2006 tsunami as an example.

For this purpose, a tsunami simulation was separately applied to two different sources of bathymetry data, namely, General Bathymetric Chart of the Oceans (GEBCO) data and ETOPO1 data, and the misfit between the modeled results was evaluated. The GEBCO data contain bathymetry data with grid intervals of 15 arc seconds, while ETOPO1 data have sea depth data with a resolution of 1 arc minute. To fairly investigate the model performances from different datasets, bathymetry data from the two datasets were converted to 450 m grids and used as the input for the numerical tsunami simulations. Figure 7 Shows the bathymetry data of the modeled domain obtained from GEBCO and ETOPO1 data. As the initial condition, the initial water distribution of the tsunami generated by the proposed multiple fault model (LS2) was used for these simulations, in which the asperity locations of the two earthquakes were assumed to be at the center of the entire fault area.

2.6 Evaluation of the bathymetry effect on tsunami wave trapping

To examine any significant change in tsunami wave transmission that could be attributed to the bathymetry effect during the passage of the 2006 tsunami, numerical experiments (MS, EXP1, EXP2) for tsunami propagation were conducted using actual and manipulated bathymetry data. For the main simulation (MS) numerical experiment, actual GEBCO bathymetry data with a resolution of 450 m derived from sea depth data with grid intervals of 15 arc seconds were used. For the manipulated bathymetry data that were used for numerical experiment EXP1, sea depths greater than 500 m were replaced with 500 m depths. For numerical experiment EXP2, the bathymetry data were manipulated by removing sea depth data with a flattened sea bottom at a depth of 500 m. The 500 m depth was specified because the bathymetric slopes are very gentle at sea depths shallower than 500 m near southern Taiwan, and the area is therefore considered a shelf region. Figure 8 Shows the map-manipulated bathymetry of the model domain for numerical experiments EXP1 and EXP2. The details of the bathymetry data used for numerical experiments MS, EXP1, and EXP2 are summarized in Table 5.

The results of the numerical experiments were compared to examine how tsunami wave directivity could change due to the bathymetric effect and to evaluate how much tsunami wave energy could be coastally trapped in different bathymetric conditions during the passage of the 2006 tsunami.

5. Sensitivity analyses of source models and bathymetry data

5.1 Single fault models

5.1.1 Tsunami sensitivity to fault depths

The sensitivity of simulated tsunami waveforms to fault depth was evaluated by varying the central fault depths of the first earthquake. Fault dimensions of 40 km × 20 km were applied to the two earthquakes. The single fault model of the two earthquakes was constructed using the GCMT solution of nodal plane NP2 for the first earthquake and NP1 for the second earthquake. The tide gauge stations of Dongkung and Houbihu were chosen for this sensitivity analysis because they the closest stations to the source region and were therefore more sensitive to the tsunami source. The single fault models of the two earthquakes and the locations of the near-field tide gauge stations that were used for the sensitivity analysis of fault depths are shown in Figure 14a.

Figure 14b shows the observed and simulated tsunami waveforms at the Dongkung and Houbihu stations using different fault depths of the first earthquake. At the Dongkung station, the first circle of simulated tsunami waveforms matched the observed data well regardless of the fault depths. At the Houbihu station, the first wave crest of the simulated waveform from a fault depth of 35 km was half the size of the observed value. Simulated tsunami waveforms with shallower depths of 15 km and 20 km produced significantly higher amplitudes during the arrival of the first crest wave. These results revealed that coastal sites with a shorter distance to the source are more sensitive to earthquake fault depths. The simulated waveforms from a central fault depth of 20 km fit the observed data better than other simulations did, and therefore, this was considered the best fault depth for simulation.

5.1.2 Comparison of eight models

Single fault models with fault dimensions of 40 km × 20 km and central depths of 20 km for the first earthquake and 33 km for the second earthquake were used in tsunami simulations using eight different sets of focal mechanisms for the two earthquakes estimated from GCMT and USGS data. The single fault models of the two earthquakes with different focal mechanisms are plotted in Figures 15 and 16. The details of the eight different sets of earthquake focal mechanisms are listed in Table 7.

In general, the simulated tsunami waveforms from all eight sets of earthquake focal mechanisms matched the observed data well. Figure 17 shows the observed and simulated tsunami waveforms at the Dongkung and Houbihu stations using the eight different sets of earthquake focal mechanisms. The simulated tsunami waveform from the earthquake focal mechanisms of S3 (misfit = 0.530), S5 (misfit = 0.529), and S7 (misfit = 0.493) showed a better fit to the observations than did the other simulations (Table 7). Among them, the earthquake focal mechanisms of S7 were found to be the best fitting scenario with the smallest misfit from the observations. Scenario S7 contained the fault orientations of NP2 for the first earthquake and NP1 for the second earthquake from USGS's moment tensor solution (Figures 15d, 16c).

While the single fault models can produce simulated tsunami waveforms that are consistent with the observations, the poorly sampled (i.e., 6 min interval) signals recorded at the coastal stations also raised some questions, as one would expect some potential high tsunami waves behind the observed signals. To that sense, overestimation of the modeled results was expected, but the simulated tsunami waveforms using single fault models presented the opposite results. This indicates that the single fault models (i.e., with uniform fault slip) may not be sufficient and that the asperity area (i.e., with a large fault slip) on the fault should be evaluated. The tsunami sensitivity to asperity locations of multiple fault models are discussed in the next section.

5.2 Tsunami sensitivity to uniform and non-uniform fault slip models

The sensitivity of simulated tsunami waveforms to non-uniform fault slip distribution was evaluated based on the best fitting fault geometry of S7. The fault model with uniform slip was also modeled to identify the significant differences in the modeled results from the uniform and non-uniform slip fault models.

Figure 18 shows the observed and simulated tsunami waveforms at the Dongkung and Houbihu stations using non-uniform slip models (9 cases in total) and a uniform slip model. At the Dongkung station, the simulated tsunami waveforms from multiple fault models were not much different from those of the single fault models. Both models could produce tsunami waveforms in good agreement with the observed values recorded at this station. At the Houbihu station, the non-uniform slip models produced a significantly higher first wave crest than the observations. The simulated wave peaks from the non-uniform slip models produced wave heights approximately twice those simulated using the uniform slip. These results indicated that the near-field station of Houbihu was rather sensitive to the effect of the fault slip distribution, and some high tsunami waves might have been missing from the recorded signals at the Houbihu station during the 2006 tsunami.

5.3 Tsunami simulation using open-source bathymetric data

To analyze the tsunami sensitivity on different sources of open-source, accessible bathymetry data, numerical simulations were applied using GEBCO and ETOPO1 data. The differences between the modeled results using these different bathymetry data were evaluated to compare the modeled wave peaks and waveforms in the 2006 tsunami.

Figures 19a and 19b show the spatial distribution of the maximum wave heights simulated using two bathymetric grids, the GEBCO data and ETOPO1 data. To evaluate the differences between the modeled wave peaks, the variation and percent change in the variation were calculated, which can be defined in equations (12) and (13):

$$Var_{peak} = Peak_{GEBCO} - Peak_{ETOPO1} \tag{12}$$

$$\% \, Var_{peak} = \frac{Peak_{GEBCO} - Peak_{ETOPO1}}{Peak_{GEBCO}} \times 100 \tag{13}$$

where Var_{peak} is the variation in the modeled wave peaks calculated at each computational grid with GEBCO and ETOPO1 data and $Peak_{GEBCO}$ and $Peak_{ETOPO1}$ are defined as the calculated wave peaks of progressive waves in a unit area of the free surface. Figures 19c and 19d illustrate the spatial distribution of the variation and percent change in the variation of the modeled wave peaks in the model domain, indicating the differences in the modeled results using the two bathymetries. The results suggested that the variation in the modeled wave peaks using the two bathymetries was greater than 0.05 m and the percent change was greater than 50% between the modeled results for areas with sea depths of less than 500 m.

Figure 20 shows the modeled tsunami waveforms at the three coastal stations (i.e., black circles in Figure 19) using the two bathymetric grids. At Kaohsiung, the modeled waveforms from the two bathymetries matched each other well; however, the modeled wave peak from the ETOPO1 data was significantly smaller than that from the GEBCO data. The bathymetries from the GEBCO and ETOPO1 data could produce tsunami waveforms at Dongkung and Houbihu that were similar in both wave periods and peaks. Table 8 summarizes the details of the coastal stations and the peak variation percentage of the modeled results from the two bathymetries.

6. The mechanism of tsunami wave trapping

6.1 Bathymetry effect on tsunami wave directivity

It is commonly understood that tsunami velocities are mainly governed by seafloor depths. A tsunami propagates at a slower speed when the tsunami wave enters shallow water from deeper water. The significant change in propagation speed allows the tsunami to change its wave direction. To assess the bathymetry effect on tsunami wave directivity during propagation, simulations were applied using actual (MS) and manipulated bathymetry experiments (EXP1 and EXP2).

Simulated snapshots of tsunami wave propagation using actual (MS) bathymetry data are shown in Figure 21. The continental shelves in front of Hengchun Peninsula have shallow depths compared to the open ocean. Figures 21a and b present how tsunami waves repeatedly changed their directions among the shelves and then refracted into the west coast embayment. The tsunami waves were reflected from the coast after arrival and tended to radiate offshore. However, they did not fully radiate offshore; instead, they were reflected again at the boundary of the shelf and refracted north toward Kaohsiung and Dongkung (Figure 21c, d). The high-energy waves repeatedly reflected and refracted among the shelves. Only rare tsunamis were transmitted back to the open ocean or to the east coast. These results indicated that the tsunami waves were trapped over the shelves during their passage in the 2006 tsunami event. Due to this fluctuation, the high-energy tsunami wave remained along the western coast for a long time, which could be clearly seen at 75 min and 90 min after the occurrence of the first earthquake (Figure 21e, f).

Figure 22 shows snapshots of the simulated tsunami wave propagation using manipulated (EXP1) bathymetry. In this situation, the transmission of tsunami waves in the shallow area was similar to those simulated using the actual (MS) bathymetry, in which the tsunami waves were persistent and repeatedly reflected and refracted among the shelves, but more reflected waves from the coast radiated to the open sea (Figure 22b-f). This is because the tsunami source was located in an area with sea depths over 500 m, and bathymetry data with sea depths over 500 m were replaced with a 500 m depth in this hypothetical situation.

Aside from the numerical experiment EXP1, a rather hypothetical situation (EXP2) was conducted to simulate tsunami wave propagation on a bathymetry with a flat sea bottom and a sea depth of 500 m. Figure 23 shows snapshots of simulated tsunami wave propagation using the manipulated (EXP2) bathymetry. An inspection of the tsunami wave transmission in the shallow area indicated that the reflected tsunami waves from the coast radiated homogeneously offshore, and the wave reflection and refraction could not be clearly seen. In addition, the tsunami waves propagated at a rather fast speed (i.e., in comparison to MS and EXP1) and mostly radiated out of the model domain at 75 min and 90 min after the occurrence of the first earthquake (Figure 23 d, e).

6.2 Tsunami wave energy trapped on the shelf

While the past section specified that tsunami waves are trapped over shelves due to the wave directivity change associated with the configuration of coastal bathymetry, the question remains of how much wave energy can be trapped over the shelves in front of southern Taiwan during the passage of tsunamis. To quantitatively evaluate the wave energy trapped over the shelves, the trapped ratio was used to indicate the tsunami energy trapped in bathymetric situations, as calculated in equation (14):

$$R_T = \frac{E_{Shelf}}{E_{Total}} \times 100 \tag{14}$$

where R_T is the ratio of tsunami energy trapped, E_{Shelf} is the calculated tsunami potential energy on the shelves (i.e., shallow areas with sea depths under 500 m), and E_{Total} is the calculated total tsunami potential energy of the model domain at each time step. The tsunami potential energy was determined assuming that the energy flux of the tsunami wave progressed in a unit region of the free sea surface (Nosov et al., 2014) and was determined using equation (15):

$$E_p = \oiint \frac{1}{2}\rho g \eta^2 \, dx \, dy \tag{15}$$

where E_p is the tsunami potential energy, ρ is the water density of the ocean, g is the gravitational acceleration (set as 9.81 m s^{-2}), and η represents the surface integral of the ocean surface disturbance at each time step. The ratio of trapped tsunami energy was calculated from the snapshots of tsunami simulations using actual (MS) and manipulated (EXP1 and EXP2) bathymetry. Figure 24 shows the calculated trapped ratio from simulated tsunami propagation snapshots every 15 min using actual (MS) and manipulated (EXP1 and EXP2) bathymetry. Note that for calculating the trapped ratio from simulations using manipulated bathymetry (EXP1 and EXP2), the shelf region corresponding to the actual bathymetry (MS) was used (i.e., the shallow area illustrated by the solid and dashed black lines shown in Figures 22 and 23). According to equations (14) and (15), the simulations yielded a ratio of trapped tsunami energy of more than 50% when using actual bathymetry (MS) and manipulated bathymetry (EXP1) but a smaller trapped ratio of 20% when using manipulated bathymetry (EXP2). These results quantitatively provided another confirmation that the coastally trapped tsunami wave energy was related to the shape of the bathymetry.

6.3 Comparison of simulated tsunami waveforms

To understand any significant change in tsunami waveforms that can be recognized with and without wave trapping, tsunami waveforms simulated from actual (MS) and manipulated bathymetry (EXP1 and EXP2) were compared. Figure 25 shows the simulated tsunami waveforms at the three coastal stations in southern Taiwan using actual and manipulated bathymetry.

Using the manipulated bathymetry (EXP1), the first few circles of simulated tsunami waveforms at all the stations were consistent with those simulated using actual bathymetry (MS) but produced slightly smaller later phase amplitudes. An inspection of the simulated waveforms using the manipulated bathymetry (EXP2) indicated an earlier arrival time of the first wave and smaller amplitudes of the later phase than those of the simulation results using actual (MS) bathymetry. These results indicated that the persistent high-energy waves along the south coast of Taiwan were associated with the mechanism of tsunami wave trapping.

6.4 Amplified and persistent high-energy waves along the coast

As described in the previous sections, the tsunami wave was trapped over the shelves and transmitted along the coast as edge waves during the 2006 tsunami. This section describes how tsunami waves behave as edge waves and to what extent such wave fluctuations influence the amplified and persisting high-energy waves along the south coast of Taiwan. Figure 26 shows the shelves in front of south Taiwan and the simulated tsunami heights of the 2006 tsunami from the main simulation (MS).

To study the behaviors of edge waves along the south coast during the 2006 tsunami, a time-distance diagram of tsunami waves is shown. Figure 27a shows the time-distance diagram of the tsunami wave along the contour of the 20 m sea depth (i.e., dashed black line in Figure 26a). Based on the phase shift of the tsunami wave, the propagation path and the travel time curve of edge waves were illustrated (i.e., green arrow in Figure 27a). According to the travel time curve, the edge waves propagated along the coast at a speed of 50 m s^{-1}. The edge waves propagated along the coast and were iteratively reflected at the shelf edge. The coupling of the edge waves and the later-arriving incident waves amplified the tsunami waves and maintained the wave oscillation in the later phase. These were visible from simulated tsunami waveforms at numerical wave gauges C and E, as shown in Figure 27c.

To understand the persisting high-energy waves along the south coast of Taiwan during the 2006 tsunami, the decreasing tendency of the tsunami wave energy along the 20 m sea depth contour was analyzed. The temporal tsunami wave energy was first determined using equation (11) and then normalized according to the maximum temporal tsunami energy in the time series. Figure 27b shows the time-distance diagram of the normalized tsunami energy along the 20 m sea depth contour (i.e., dashed black line in Figure 26a). Figure 27d shows the normalized tsunami energy at numerical wave gauges C and E. At the numerical wave gauge C, the normalized tsunami energy achieved its greatest value at approximately 40 min after the first earthquake occurred. However, this high-energy channel did not decrease with time after the first wave arrived; instead, a persisting channel of strong energy was visible. This energy channel lasted for more than 60 min, and the wave energy repeatedly reached the maximum value in this channel. Beyond this channel, the energy commenced to decrease with a rate of energy loss of 50% at 110 min and 20% at 270 min after the occurrence time of the first earthquake. At the numerical wave gauge E, the normalized tsunami energy achieved its greatest value approximately 30 min and 120 min after the first wave arrived. Beyond this channel, the energy commenced to decrease at a rather fast rate of energy loss of 80% at 150 min and 70% at 215 min after the occurrence time of the first earthquake. Accordingly, the tsunami decay process in this region was expected to last for more than 300 min. These results indicated that the wave amplification and persistent high-energy waves along the coast during the 2006 tsunami were connected to tsunami wave trapping and the influence of edge waves. According to these behaviors, southern Taiwan could be affected by intensified coastal hazards and severe impacts from tsunamis.

Table 1. Calculation conditions for the numerical tsunami simulation.

	Calculation condition for the numerical tsunami simulation
Governing equation	Two-dimensional nonlinear shallow water equations (TUNAMI-N2 model)
Numerical integration method	Leap-frog finite difference method
Initial condition	Initial water level calculated form fault parameters using the theory of Okada, 1985 considering the contribution of horizontal coseismic displacement
Coordination system	Cartesian coordinate system
Boundary condition	Radiation boundary condition
Stability criterion	Courant–Friedrichs–Lewy (CFL) condition
Time interval	0.1 s
Mesh size	450 m
Mesh number (x, y)	(538, 631)

Table 2. Focal mechanisms for successive earthquakes estimated by GCMT and USGS.

		Earthquake 1		Earthquake 2	
		NP1	NP2	NP1	NP2
GCMT	Long (º E)	120.52		120.4	
	Lat (º N)	21.81		22.02	
	Strike (deg)	165	329	151	61
	Dip (deg)	30	61	48	90
	Rake (deg)	-76	-98	0	138
	Depth (km)	20		33	
USGS	Long (º E)	120.55		120.49	
	Lat (º N)	21.8		21.97	
	Strike (deg)	171	319	151	61
	Dip (deg)	24	69	48	90
	Rake (deg)	-61	-102	0	138
	Depth (km)	25		33	

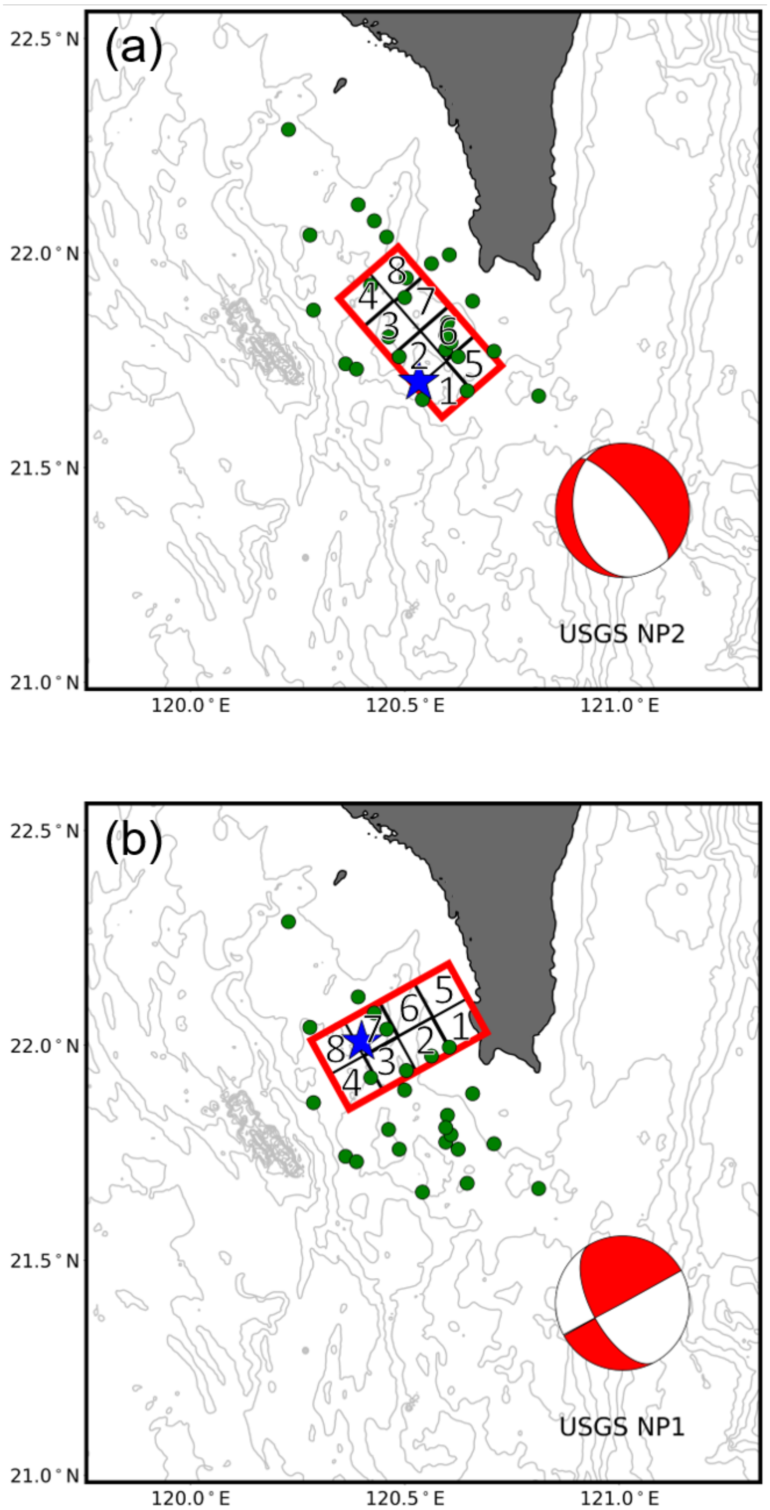

Figure 4. Fault models for the two earthquakes. (a) Subfault locations of the first earthquake (M_w 7.0) using NP2 of USGS's moment tensor solution. (b) Subfault locations of the second earthquake (M_w 6.9) using NP1 of USGS's moment tensor solution.

Table 3. Parameters of the subfaults for the two earthquakes of the 2006 earthquake doublet.

	Sub fault	Long (° E)	Lat (° N)	Length (km)	Width (km)	Depth (km)	Strike (°)	Dip (°)	Rake (°)
Earthquake 1	1	120.619	21.588	10	10	15.3	319	69	-102
	2	120.556	21.657	10	10	15.3	319	69	-102
	3	120.492	21.724	10	10	15.3	319	69	-102
	4	120.429	21.792	10	10	15.3	319	69	-102
	5	120.692	21.648	10	10	24.7	319	69	-102
	6	120.629	21.716	10	10	24.7	319	69	-102
	7	120.565	21.784	10	10	24.7	319	69	-102
	8	120.501	21.852	10	10	24.7	319	69	-102
Earthquake 2	1	120.726	21.989	10	10	29.1	151	48	0
	2	120.642	21.946	10	10	29.1	151	48	0
	3	120.557	21.902	10	10	29.1	151	48	0
	4	120.473	21.858	10	10	29.1	151	48	0
	5	120.680	22.068	10	10	29.1	151	48	0
	6	120.595	22.024	10	10	36.5	151	48	0
	7	120.510	21.980	10	10	36.5	151	48	0
	8	120.426	21.936	10	10	36.5	151	48	0

Table 4a. Details of the average slip, large slip, and background slip for the two earthquakes.

	Earthquake 1	Earthquake 2
Moment magnitude (M_w)	7.0	6.9
Entire fault size (km^2)	800	800
Rigidity (GPa)	30	30
Average slip D_a (m)	1.66	1.17
Large slip $2D_a$ (m)	3.32	2.35
Background slip (m)	1.11	0.78

Table 4b. Asperity locations of multiple fault models for the two earthquakes.

Scenario	Asperity location of Earthquake 1			Asperity location of Earthquake 2		
	North	Central	South	North	Central	South
LS1	○				○	
LS2		○			○	
LS3			○		○	
LS4	○			○		
LS5		○		○		
LS6			○	○		
LS7	○					○
LS8		○				○
LS9			○			○

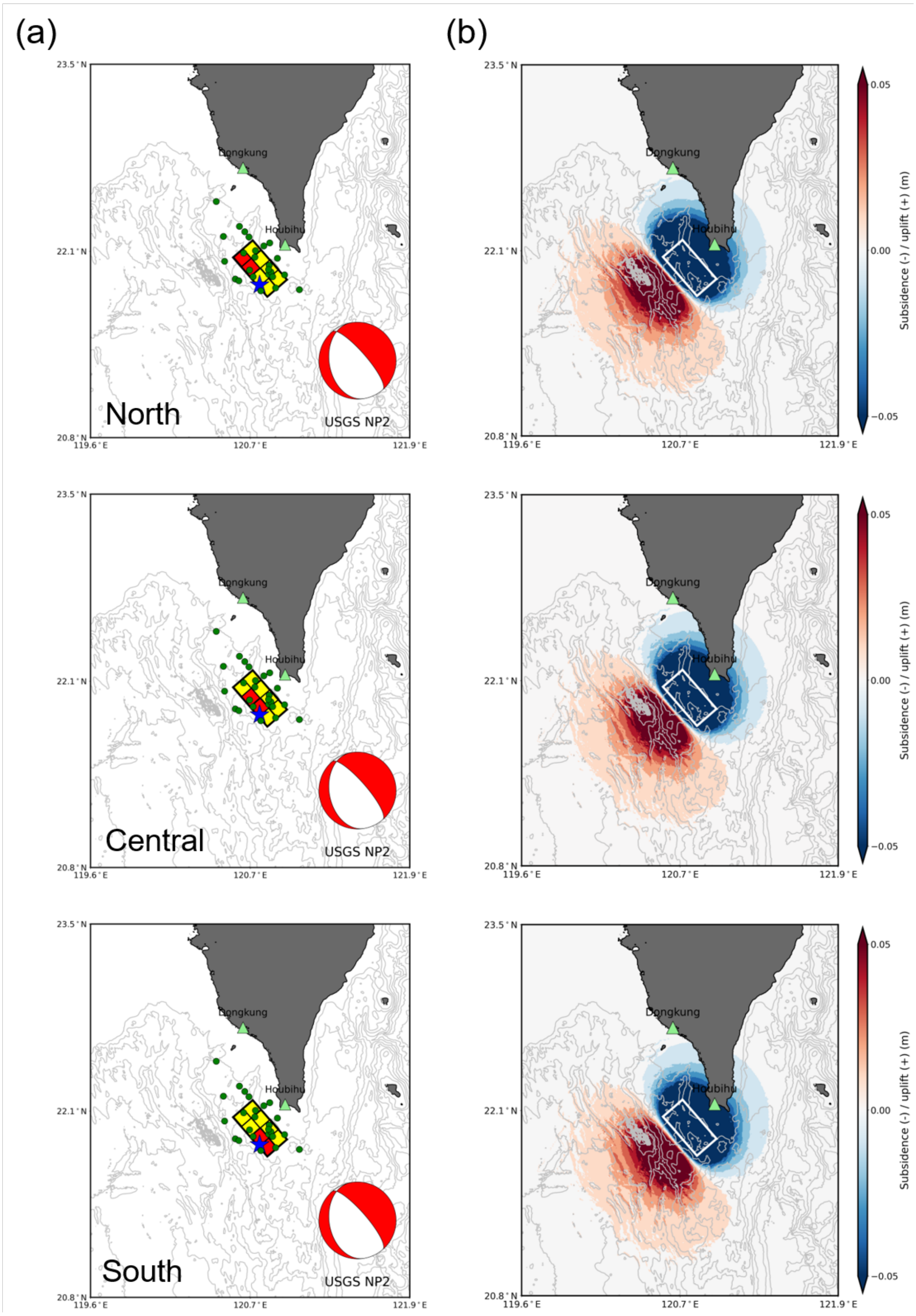

Figure 5. (a) Map of subfault boundaries with different asperity locations for the first earthquake (M_w 7.0). (b) Coseismic crustal vertical displacement calculated using the fault

parameters of the subfaults. The beachball denotes the focal mechanisms of USGS's NP2 nodal planes for the first earthquake. The subfaults in red represent large slip areas, and the subfaults in yellow represent background slip areas. The large slip area was located only at the shallow part of the entire fault area. The blue stars represent the epicenter of the first earthquake, and the green circles represent the aftershocks. The tide gauge stations are plotted as green triangles.

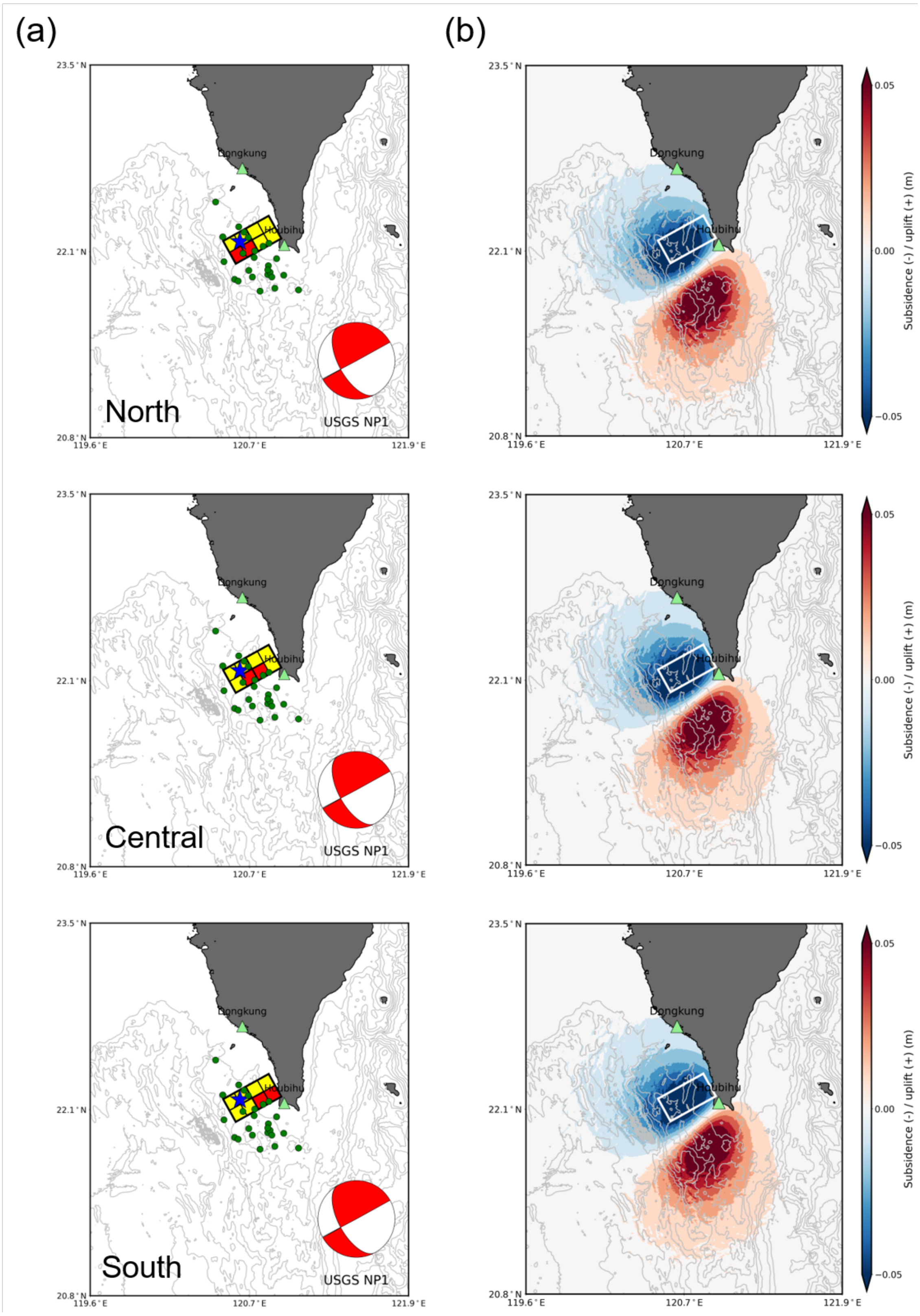

Figure 6. (a) Map of subfault boundaries with three different locations of large slip areas for the second earthquake (M_w 6.9). (b) Coseismic crustal vertical displacement calculated using the

fault parameters of the subfaults. The beachball denotes the focal mechanisms of USGS's NP2 nodal planes for the first earthquake. The subfaults in red represent large slip areas, and the subfaults in yellow represent background slip areas. The large slip area was located only at the shallow part of the entire fault area. The blue stars represent the epicenter of the first earthquake, and the green circles represent the aftershocks. The tide gauge stations are plotted as green triangles.

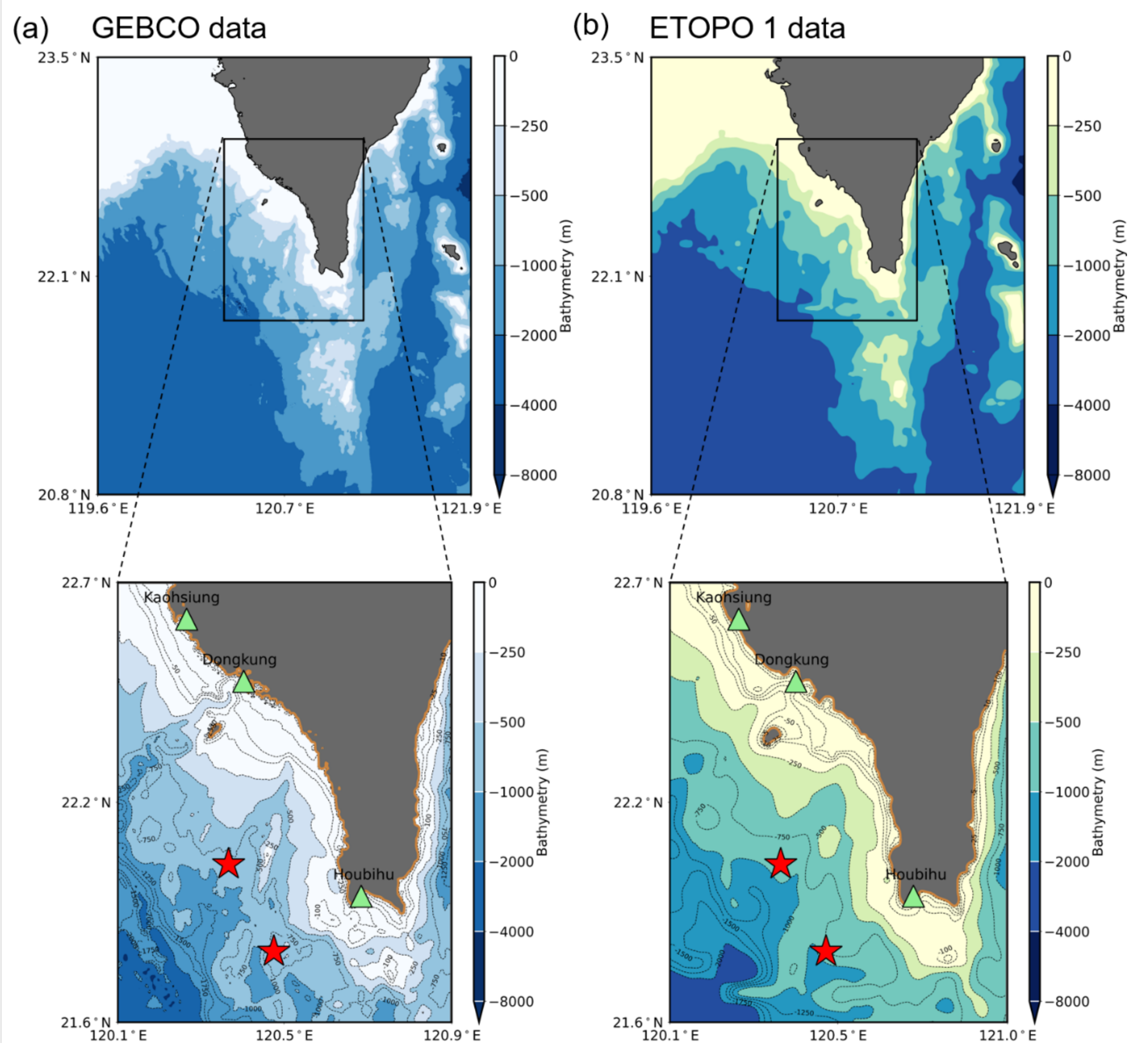

Figure 7. Bathymetry map of the model domain from GEBCO and ETOPO1 bathymetry data. The green triangles denote the locations of the tide gauge stations. The red stars represent the epicenters of the two earthquakes.

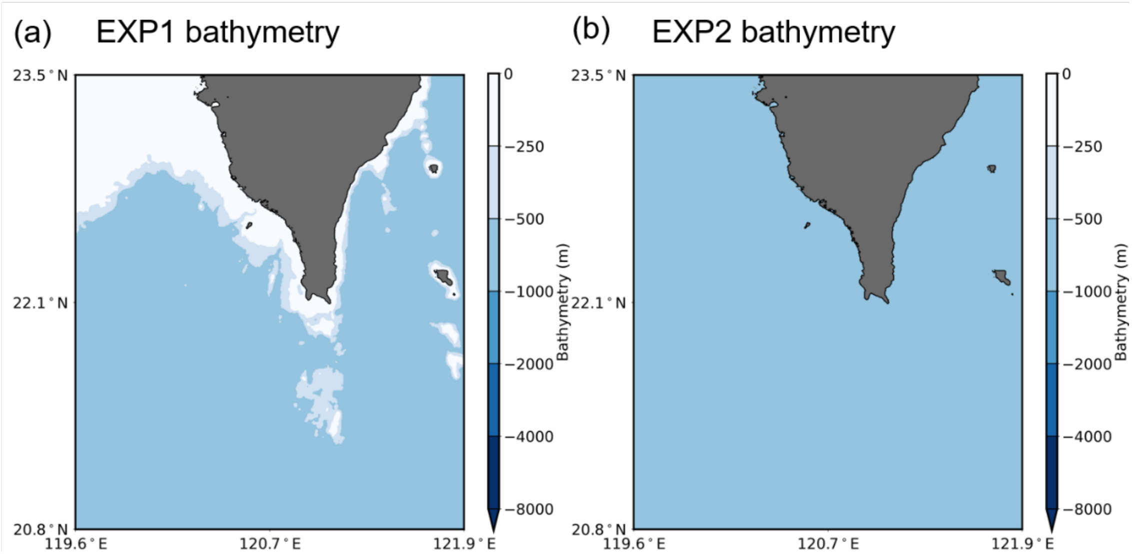

Figure 8. Maps of the manipulated bathymetry of the model domain for numerical experiments (a) EXP1 and (b) EXP2.

Table 5. Details of the bathymetry data used for the numerical experiments MS, EXP1, and EXP2.

	Numerical experiments		
	MS	EXP1	EXP2
Bathymetry source		GEBCO data	
Grid size		450 m	
Mesh number (x, y)		(538, 631)	
Description of bathymetry conditions	Sea depths from GEBCO data	Sea depths larger than 500 m were replaced with 500 m depths	Sea depths of entire domain were replaced with 500 m depths.

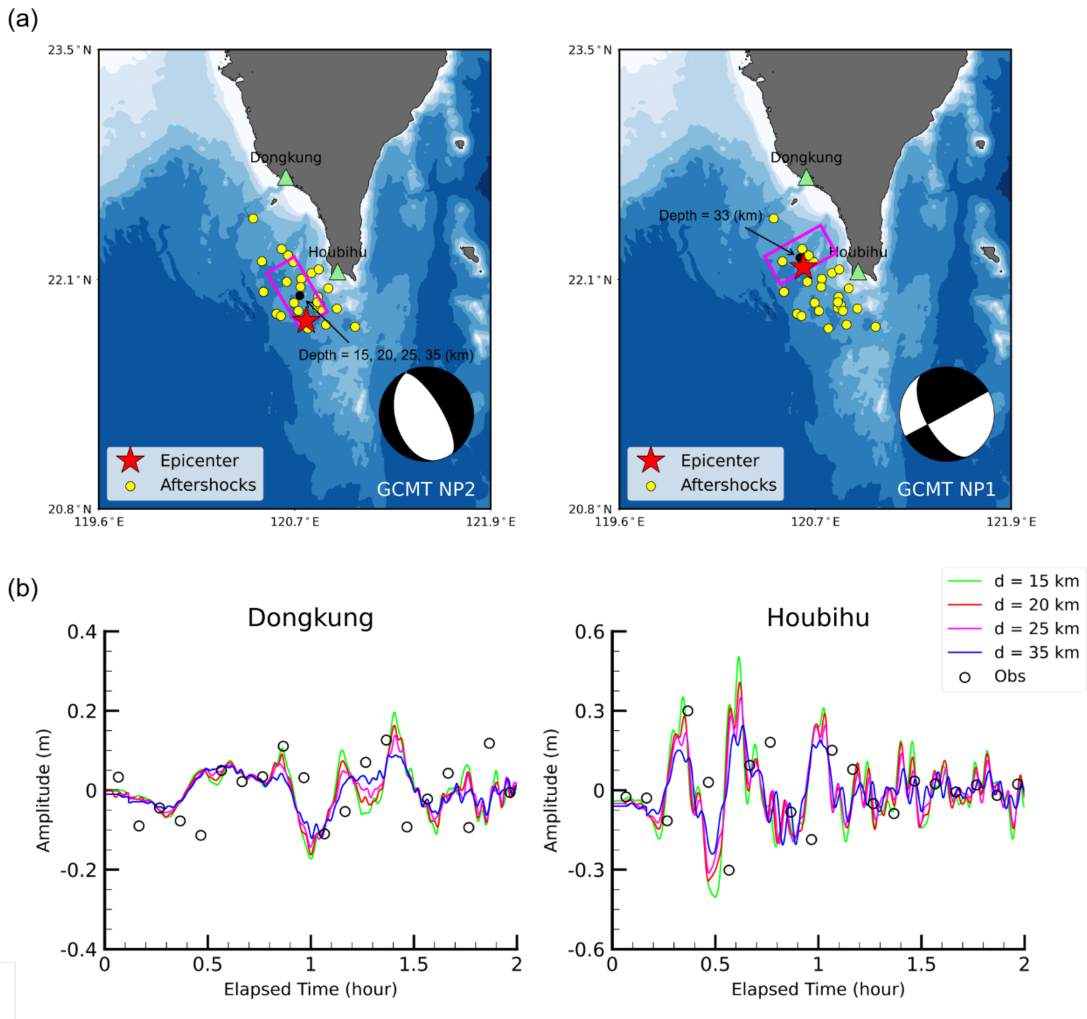

Figure 14. (a) Single fault models with fault dimensions (length × width) of 40 km × 20 km of the first earthquake using the GCMT NP2 nodal plane and the second earthquake using the GCMT NP1 nodal plane. The central fault depths of the single fault models for the first earthquake are set as 15 km, 20 km, 25 km, and 35 km, and the central fault depth is fixed at 33 km for the single fault models of the second earthquake for the tsunami sensitivity test. (b) Observed and simulated tsunami waveforms at the Dongkung and Houbihu stations using single fault models with the different central fault depths of the first earthquake.

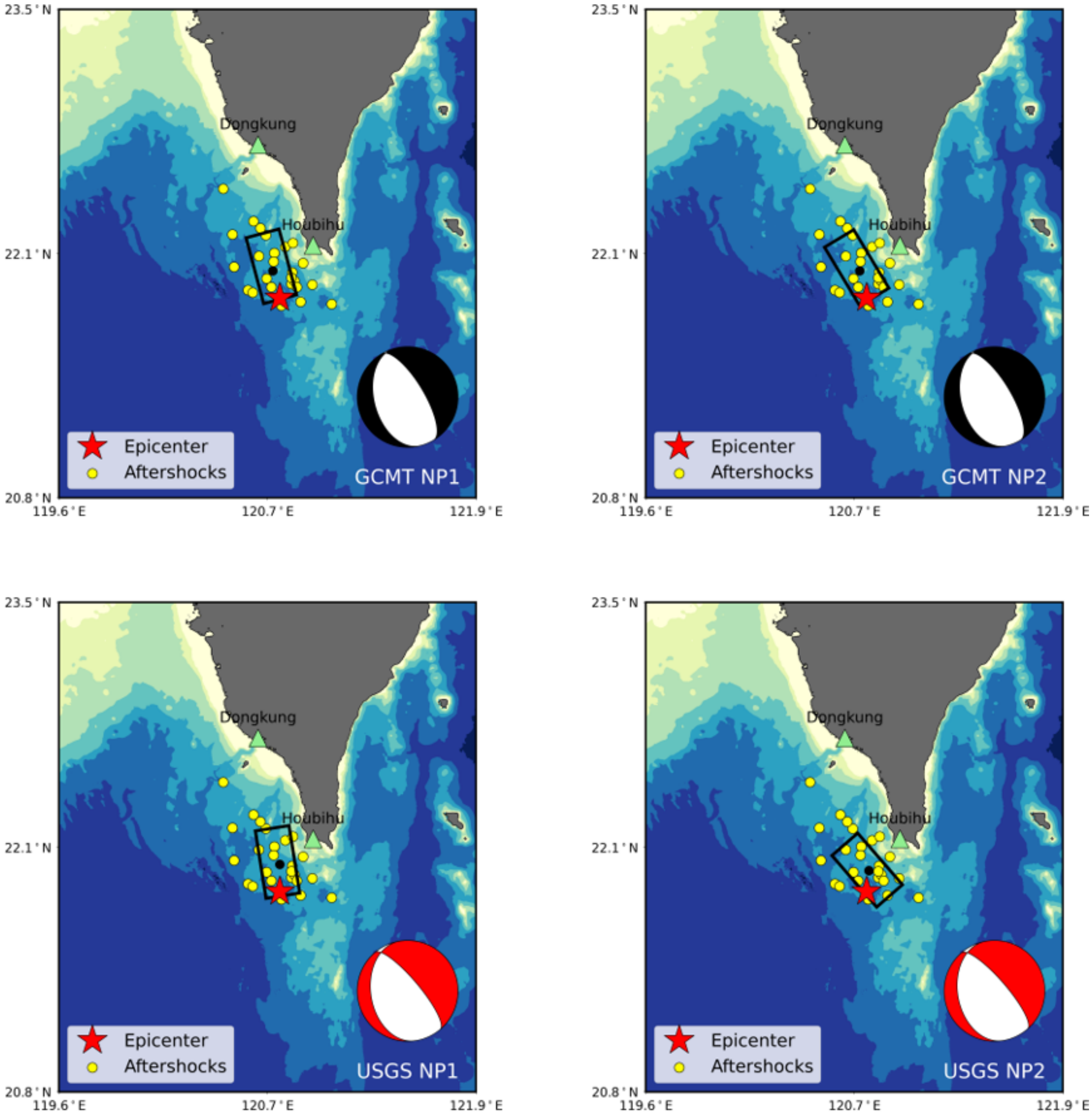

Figure 15. Simple fault models of the first earthquake (M_w 7.0) using the focal mechanisms from GCMT and USGS. The green triangles indicate the tide gauge stations, red stars indicate the epicenter, yellow circles indicate aftershocks, and the black rectangles indicate the fault model.

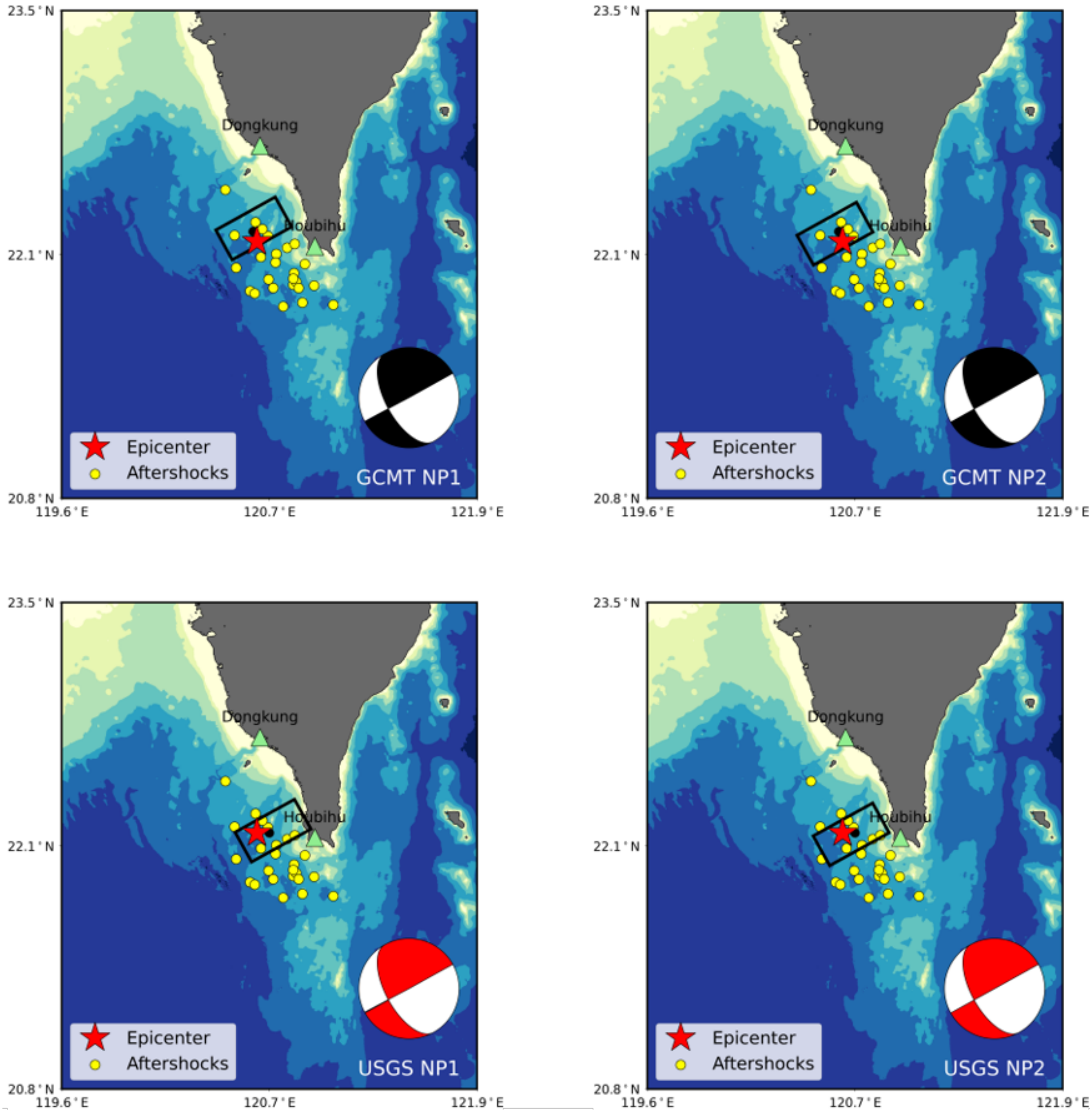

Figure 16. Simple fault models of the second earthquake (M_w 6.9) using the focal mechanisms from GCMT and USGS. The green triangles indicate the tide gauge stations, red stars indicate the epicenter, yellow circles indicate aftershocks, and the black rectangles indicate the fault model.

Table 7. Validation of the simulated tsunami waveforms using single fault models with eight different models of focal mechanisms estimated by GCMT and USGS.

Scenario	Moment tensor solution	Nodal plane		Misfit of simulated tsunami waveforms
		Earthquake 1	Earthquake 2	
S1	GCMT	NP1	NP1	0.591
S2		NP1	NP2	0.632
S3		NP2	NP1	0.530
S4		NP2	NP2	0.661
S5	USGS	NP1	NP1	0.529
S6		NP1	NP2	0.604
S7		NP2	NP1	0.493
S8		NP2	NP2	0.735

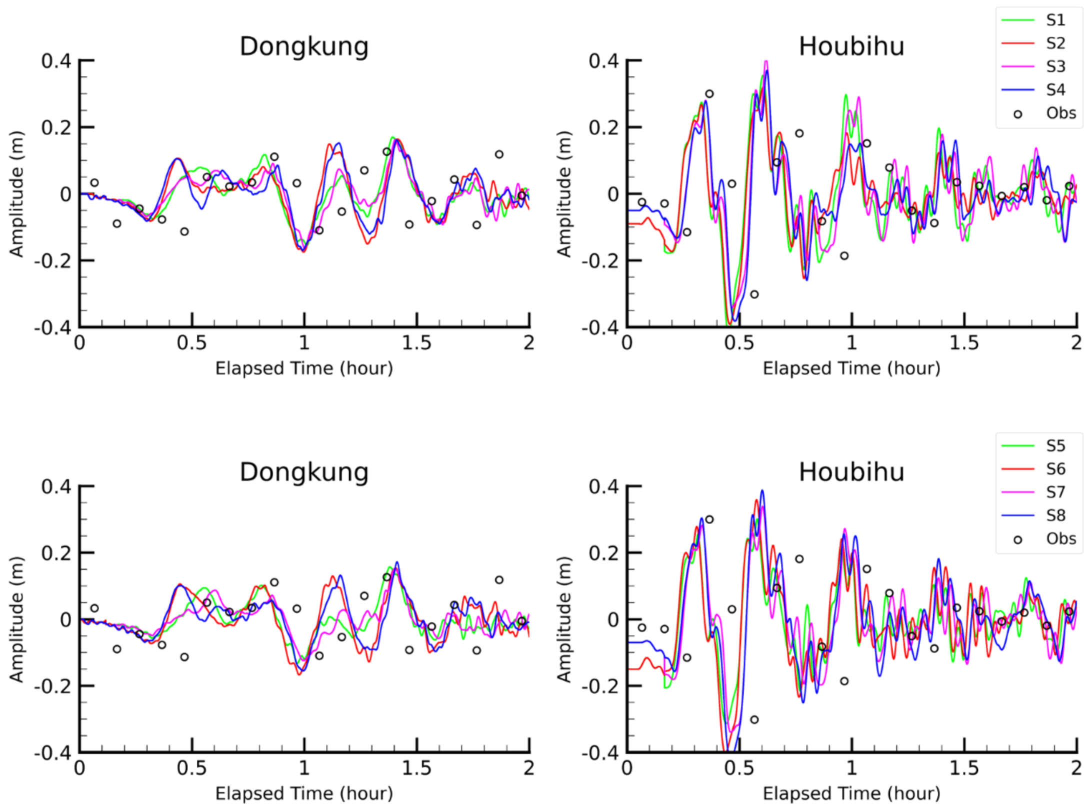

Figure 17. Comparison of simulated tsunami waveforms at the Dongkung and Houbihu stations using single fault models with eight different models of focal mechanisms estimated by GCMT and USGS.

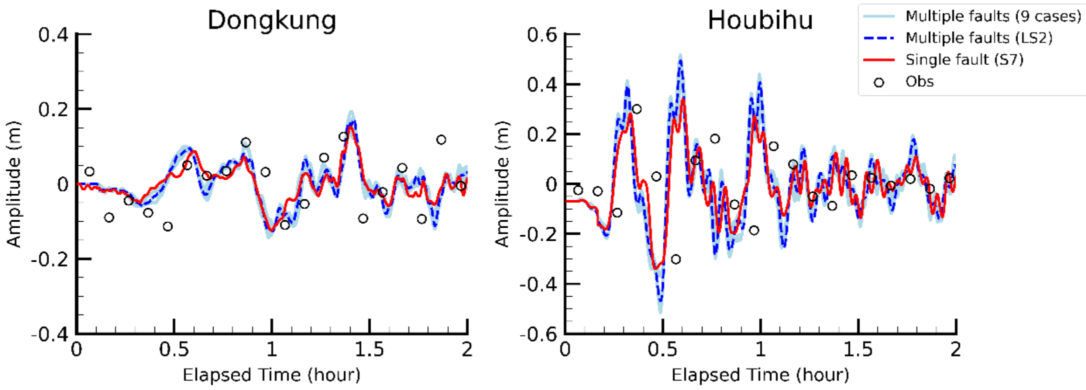

Figure 18. Comparison of simulated tsunami waveforms at the Dongkung and Houbihu stations using 9 cases of multiple fault models (solid blue lines) and a single fault model of S7 (solid red lines). The simulated tsunami waveforms using the multiple fault model (LS2) are shown as dashed blue lines. The white circles represent the observational data.

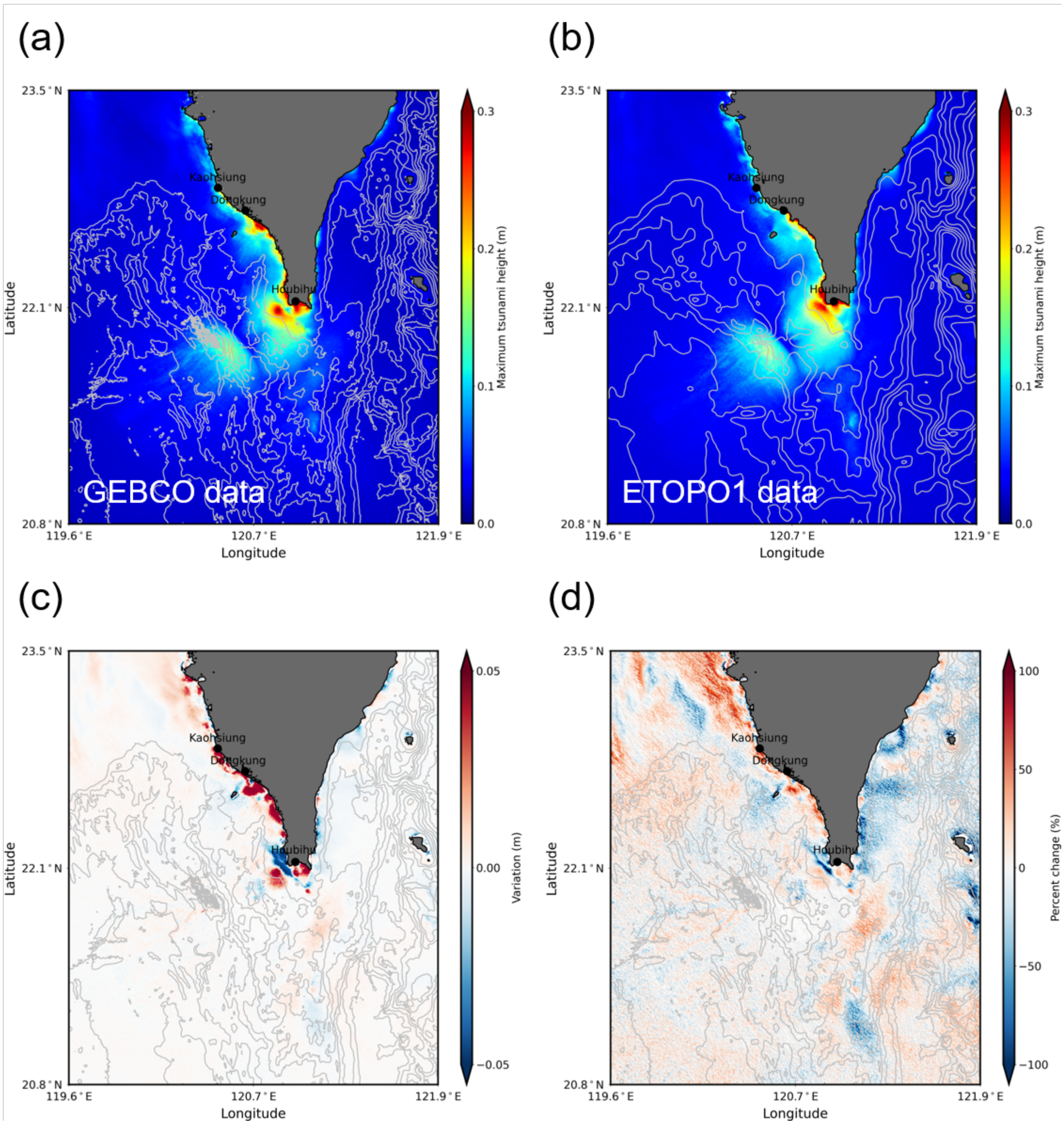

Figure 19. Simulated maximum tsunami height using open-source bathymetry data: (a) GEBCO and (b) ETOPO1 data. (c) The variation and (d) the percent variation in the simulated maximum tsunami height using two sources of bathymetry data. The black circles indicate the locations of the tide gauge stations. The bathymetry contour is 500 m based on the GEBCO or ETOPO1 bathymetric data.

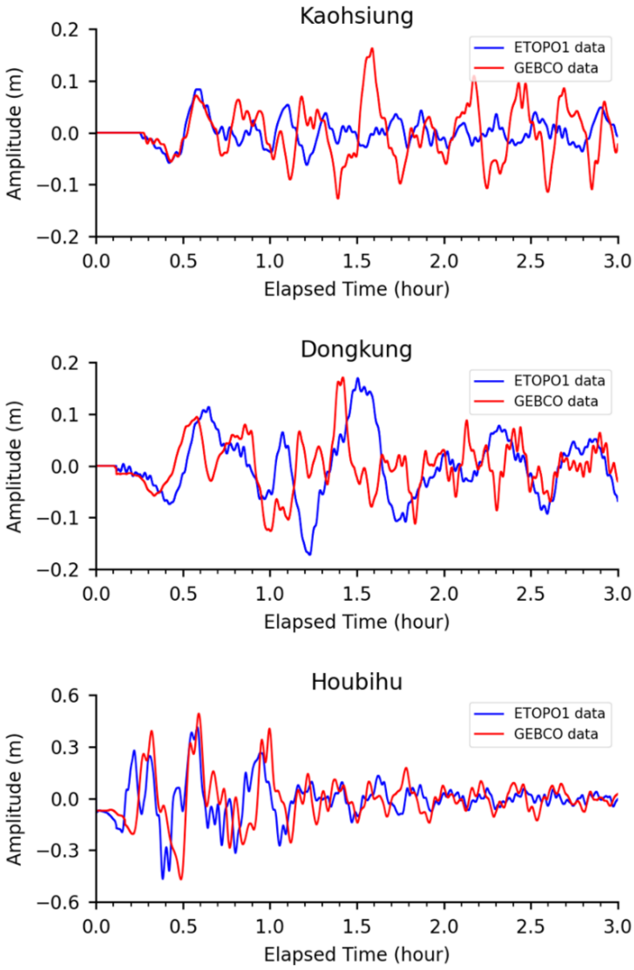

Figure 20. Simulated tsunami waveforms at the (a) Kaohsiung, (b) Dongkung, and (c) Houbihu stations using two different open-source bathymetry datasets, GEBCO and ETOPO1.

Table 8. Details of the locations of the simulated tsunami waveforms and misfit of model results using different open-source bathymetry data at three tide gauge stations.

Station	Sea depth (m)		Simulated wave peak (m)		Var_{peak}	$\%Var_{peak}$
	GEBCO	ETOPO1	GEBCO	ETOPO1		
Kaohsiung	10	8	0.163	0.084	0.079	48.45
Dongkung	9	14	0.171	0.17	0.001	0.58
Houbihu	4	11	0.493	0.414	0.079	16.02

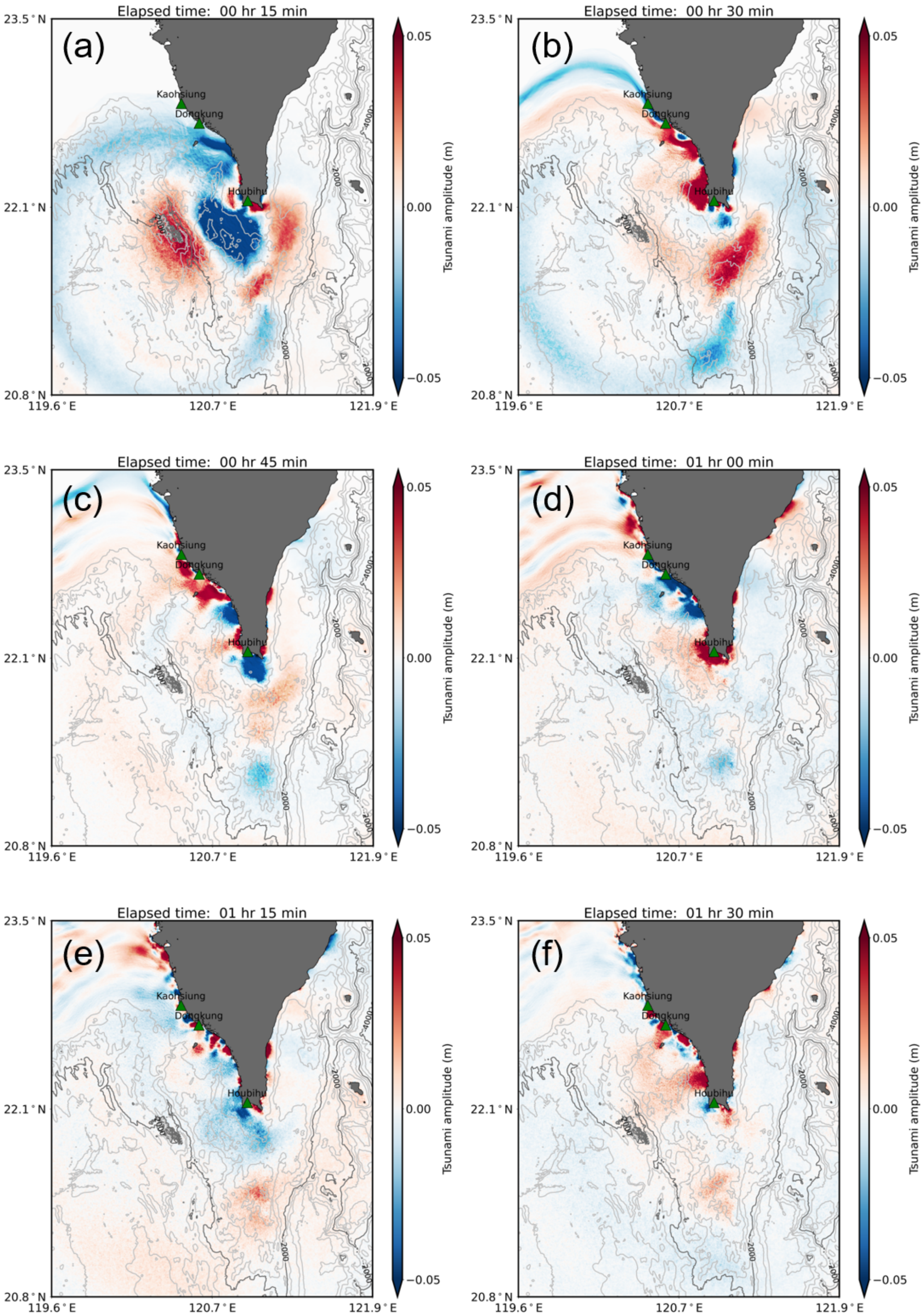

Figure 21. Tsunami propagation snapshots from the numerical experiment MS. The tide gauge stations are plotted in green triangles. The bathymetry contour is 500 m.

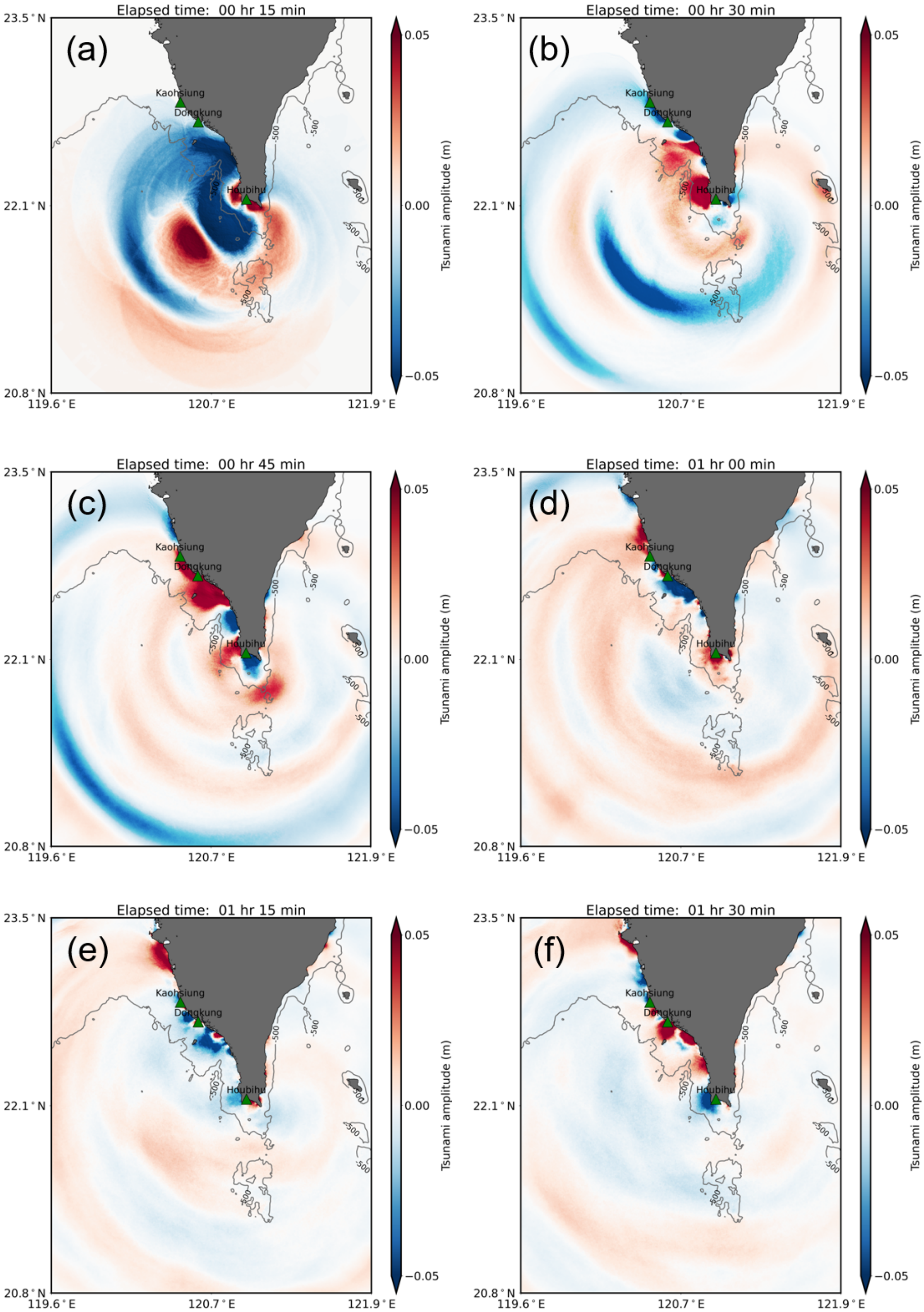

Figure 22. Tsunami propagation snapshots from the numerical experiment EXP1. The tide gauge stations are plotted as green triangles. The bathymetry contour at a depth of 500 m is shown as a solid gray line.

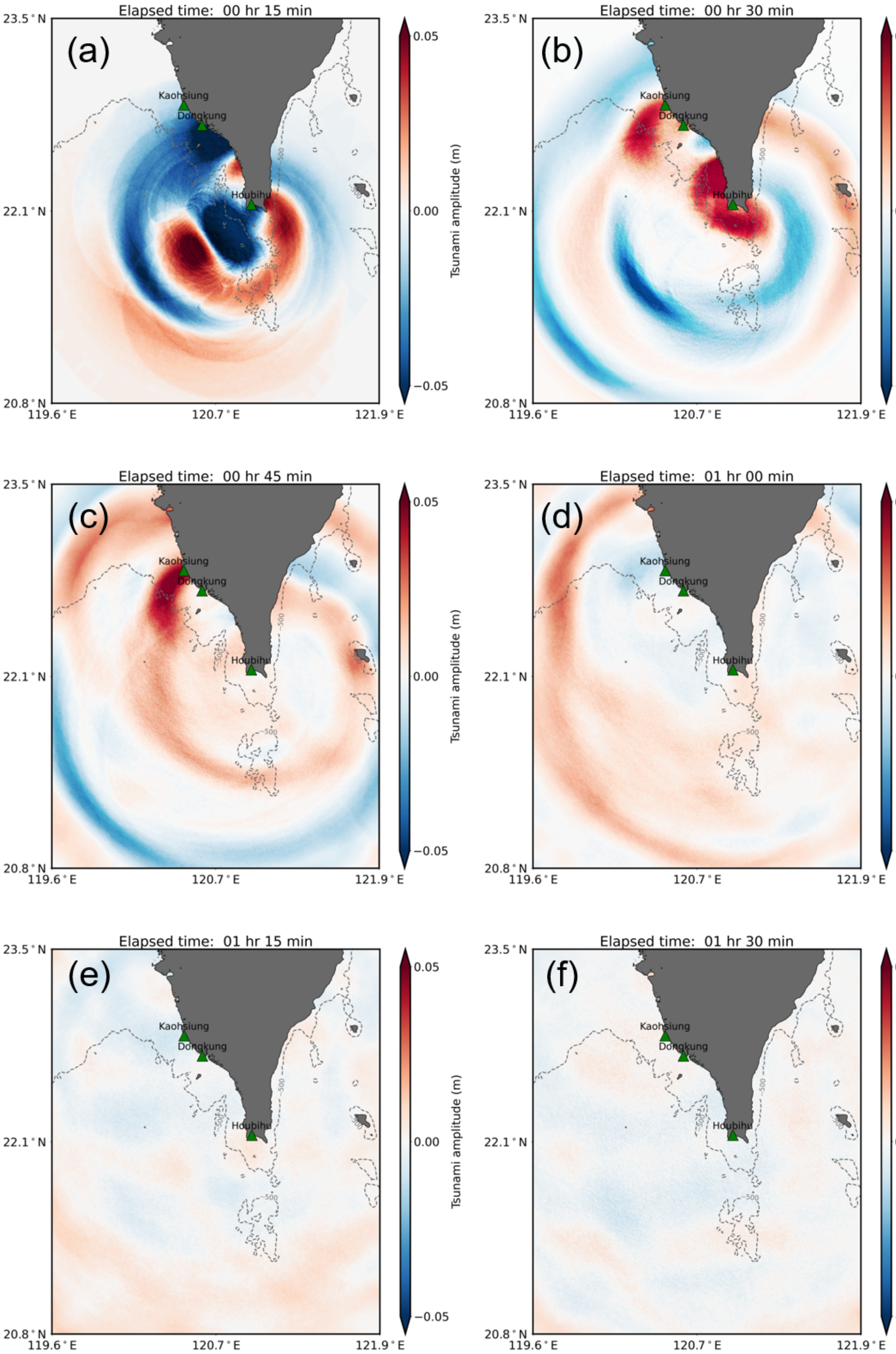

Figure 23. Tsunami propagation snapshots from the numerical experiment EXP2. The tide gauge stations are plotted as green triangles. The corresponding bathymetry contour of 500 m depth from GEBGO data is shown as a dashed gray line.

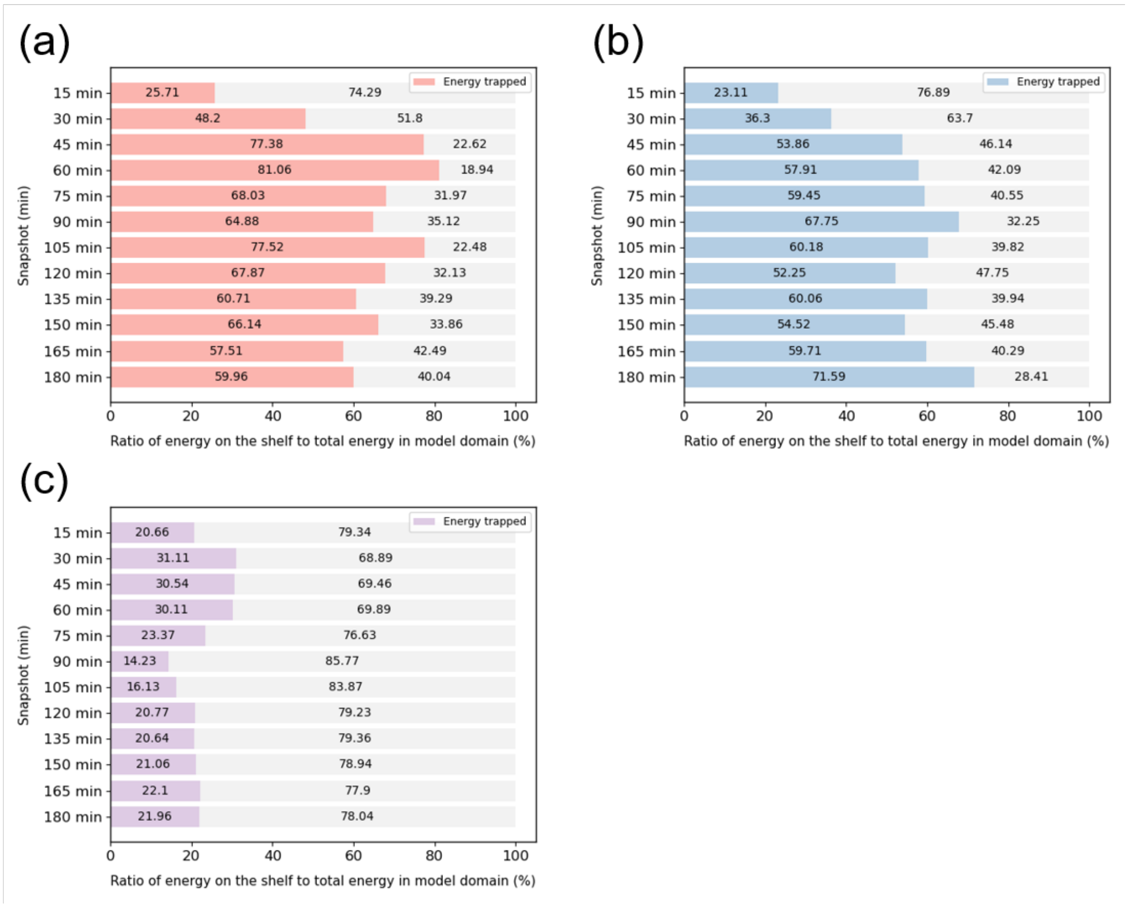

Figure 24. Trapped ratio calculated from tsunami propagation snapshots every 15 min from numerical experiments (a) MS, (b) EXP1, and (c) EXP2.

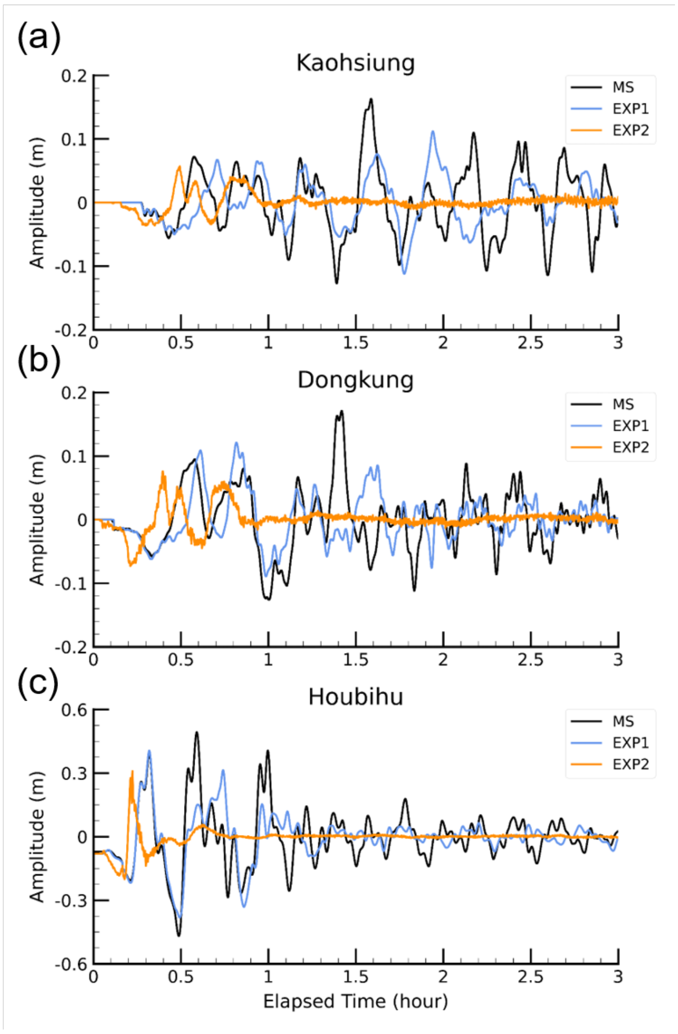

Figure 25. Simulated tsunami waveforms at the (a) Kaohsiung, (b) Dongkung, and (c) Houbihu stations from numerical experiments MS, EXP1, and EXP2.

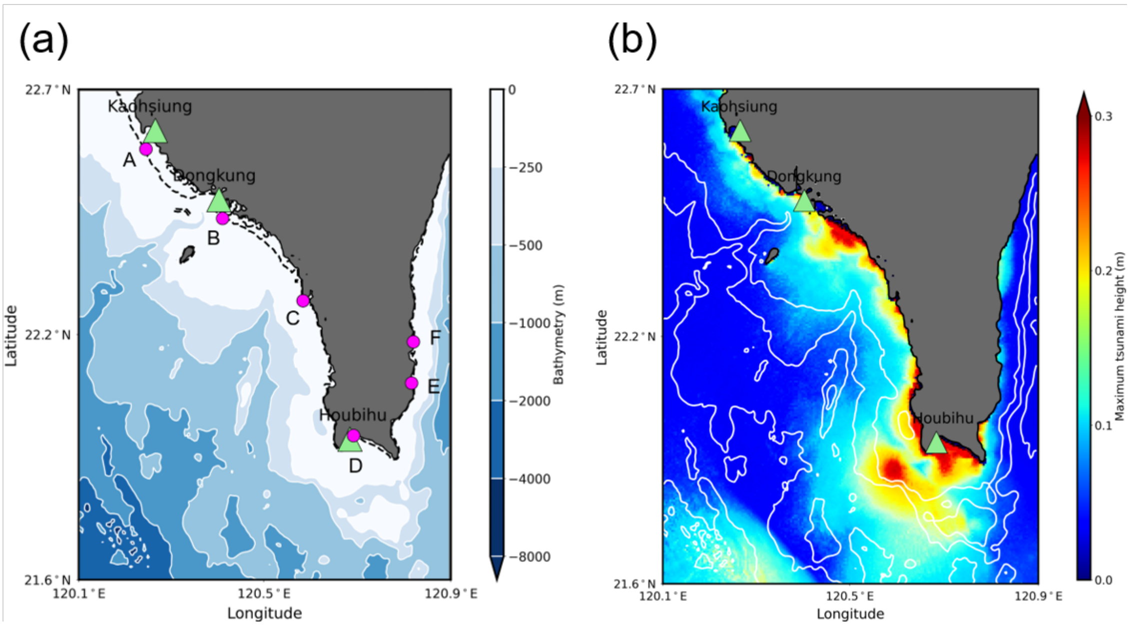

Figure 26. Zoomed map of the (a) bathymetry around southern Taiwan and (b) simulated maximum tsunami height using a multiple fault model (LS2). Green triangles indicate the locations of tide gauge stations, and pink circles denote numerical wave gauges at a sea depth of 20 m. The solid white lines are contour lines, and the dashed black line represents the bathymetric contour at a depth of 20 m.

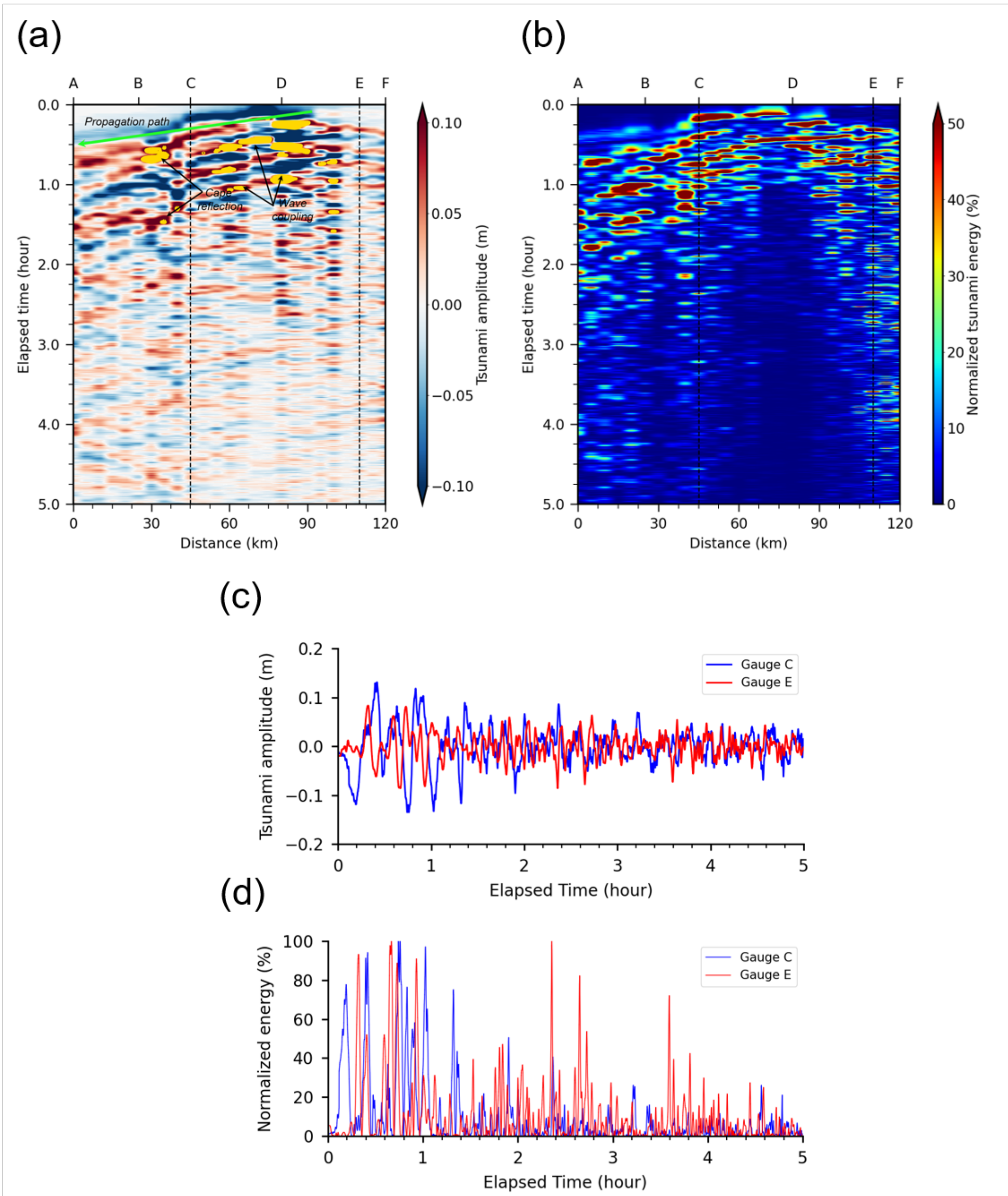

Figure 27. Time-distance diagram of the (a) tsunami wave and (b) normalized energy along the 20 m bathymetry contour from numerical wave gauges A to F and time series measurements of the (c) tsunami amplitude and (d) normalized energy at numerical wave gauges C and E. The dashed black lines indicate the distances of numerical wave gauges C and E from A. For interpretation of the references, please refer to Figure 26a.